• U C •

FCTUC FACULDADE DE CIÊNCIAS
E TECNOLOGIA
UNIVERSIDADE DE COIMBRA

DEPARTAMENTO DE
ENGENHARIA MECÂNICA

Hugoniot characterization of WC-Ni powders

Submitted in Partial Fulfilment of the Requirements for the Degree of Master in Mechanical Engineering in the speciality of Energy and Environment

Author

Rui Pedro Tavares de Sousa

Advisors

Professor José Manuel Baranda Moreira da Silva Ribeiro

Doctor João Pedro Pereira Piroto Duarte

Jury

President	**Doctor Ana Paula Bettencourt Martins Amaro** **Professor at University of Coimbra**
Vowels	**Doctor Cristina Maria Gonçalves dos Santos** **Professor at University of Coimbra**
	Doctor Ricardo António Lopes Mendes **Professor at University of Coimbra**
Advisor	**Doctor José Manuel Baranda Moreira da Silva Ribeiro** **Professor at University of Coimbra**

Institutional Collaboration

Imperial College London

Institute of Shock Physics

Coimbra, September, 2015

A arte consiste em fazer os outros sentir o que nós sentimos,
Em os libertar deles mesmos,
Propondo-lhes a nossa personalidade para especial libertação.
Fernando Pessoa, at Livro do desassossego, 1984

To my parentes and sister

Acknowledgements

I would like to acknowledge my family for the invaluable support and encouragement they have always provided me with and for always inciting me broaden my horizons. Without them on my side, neither the experiences in Coimbra, Split nor London experiences would be part of me. To my mum, dad and sister I give a heartfelt thank you.

A special thanks to Dr. William Proud for accepting me at ISP as well as to my advisor Dr. J. P. Duarte for the warm welcome and all the guidance he has been kindly offering. I shall also thanks the ISP committee, which succeeded in making me feel at home. My sincerest thanks to Professor José B. Ribeiro, for the additional advice and mentoring. Without him or Professor Cristina Santos, this collaboration between institutions would not be possible, hence I am particularly grateful to them for having given me this excellent opportunity.

Last but not least, a meaningful thank you to all my friends who have been patiently supporting me during these beautiful five years, making them more enjoyable, filled with unforgettable stories.

Abstract

Tungsten Carbide mixed with Nickel (WC-Ni) is of great importance in applications that requires high levels of hardness and wear resistance due to the combination of properties granted by the presence of two different phases: Tungsten Carbide phase imparts the hardness and the strength while metallic matrix acts to increase ductility and toughness.

The dynamic behaviour of WC-Ni powders, with Nickel content of 11% was studied under planar loading conditions. A gas gun was used to conduct planar impact experiments at velocities of 320, 500 and 620 m/s to determine the shock and wave propagation characteristics of the material stablishing the Hugoniot relations in different planes.

When the material is shocked between 1.1 to 4.8 GPa, a steady shock wave is generated which propagates at a velocity ranging from 866 to 1620 m/s and transfers energy into particles that moves at velocities between 151 and 300 m/s after its passage.

Based on the achieved results, recommendations will be made for performing future works aimed at improving the experimental technique, with the purpose of enhancing the understanding of the behaviour of materials when subjected to shock.

Keywords: Tungsten Carbide powders mixed with Nickel, Porous materials, Shock waves, Hugoniot relations, Plate impact experiments, Heterodyne velocimetry.

Resumo

O carboneto de tungsténio com adição de uma matriz secundária de Níquel (WC-Ni) é de grande importância em aplicações em que são exigidas grandes valores de resistência e abrasão. Estas propriedades são garantidas pelas diferentes fases da estrutura, em que o WC garante rigidez enquanto que o Ni adiciona plasticidade e ductilidade ao material.

O comportamento ao choque dos pós de WC-Ni (mistura com 11% de Níquel) é estudado com recurso a condições de impacto planar. Esta experiência recorre a um canhão de gás comprimido para realizar impactos a altas velocidades de projétil na ordem de 320, 500 e 620 m/s. Esta metodologia permite obter informação suficiente para caracterizar a propagação das ondas de choque no material estabelecendo a chamada relação de Hugoniot.

Quando o impacto dos corpos gera pressões entre 1,1 e 4,8 GPa, é gerada uma frente de onda de choque que se propaga a velocidades compreendidas entre 866 e 1620 m/s. A passagem da onda no material transfere energia às partículas induzindo-lhes velocidades entre 151 e 300 m/s.

Com base na análise dos resultados, são propostos trabalhos futuros para o melhoramento da metodologia experimental com o intuito de aprofundar o conhecimento do comportamento dos materiais face ao choque.

Palavras-chave: Carboneto de tungsténio misturado com níquel, Materiais porosos, Ondas de choque; Relação de Hugoniot, Impactos planares, Canhão de gás comprimido.

Contents

LIST OF FIGURES

LIST OF TABLES

SIMBOLOGY, SUBSCRIPTS AND ACRONYMS

Simbology

A – Area

c – Light speed

C_0– Velocity of sound on the material

d – Diameter

e – Internal energy

f_0 – Initial frequency of light

f_b – Frequency of beat signal

f_d –-Frequency of Doppler shifted light

m – Mass

P – Pressure

u_p – Particle velocity

U_s– Shock wave velocity

x_{sample} –-Thickness of the sample

α – Coefficient of linear thermal expansion

λ – Wavelength

ρ – Density

σ – Stress

Γ – Mie-Grüneisen parameter

ν – Specific volume

Δt – Span time

Subscripts

P – Porous material

S – Non-porous material

0 – Non- shocked material

1 – Shocked material

Acronyms

DEM – Departamento de Engenharia Mecânica

FCTUC – Faculdade de Ciências e Tecnologia da Universidade de Coimbra

HetV – Heterodyne Velocimetry

ICL – Imperial College of London

ISP – Institute of Shock Physics

1. INTRODUCTION

1.1. Background and objectives

From a basic point of view, experimental study of the dynamic behaviour of materials is rather simple. An experiment can be easily performed by introducing a stress in the material and measuring its response in terms of deformation and/or force. For low velocity impacts, the behaviour of the material is mastered by elastic wave deformation since the applied stress on it is lower than the material's yield strength. On the other hand, if it is a high velocity impact, the scenario is different. The extreme high induced pressures can exceed the strength of the material driving it into a regime that involves the propagation of elastic-plastic waves. Under these conditions, the matter has a nonlinear response and demands a deep study for an entire characterization of the propagation of waves.

The thermodynamic properties of the material allows to better understand how does the material behaves when subjected to high pressures. Two of these properties can be measured experimentally. When applying the conservation equations to both parameters, it is possible to achieve a complete characterization. Referred as Hugoniot equations, these relations are a locus of shocked states for a given material and can be used as valuable thermodynamic information at high pressures.

Tungsten Carbide (WC) is a very interesting material because of its low density and high strength when compared with the pure W. Sometimes referred to as a hard metal, this ceramic is widely used in the production of cutting tools, molds and also in the petrol industry has the constituent of drilling tools. The shock behaviour of WC has been studied throughout the years by many researchers such as McQueen (1970), Amulele (2008), Vogler (2005), and Grady (1995, 1999 and 2009) among others. However, some of this authors also studied the shock compression in several ceramic powders, finding out their excellent behaviour to shock because of their high distention, which results in very slow shock velocities.

This project focuses on measuring the relation between the velocity of the shock waves and the particle velocity in Nickel-doped Tungsten Carbide powders compacted by

isostatic pressure. In fact, these two data lead to the Hugoniot relations. The Hugoniot data, in its turn, can be used for the design of dynamic compaction procedure since the uniformity of the compaction is related to the velocity of the shock. In this case, shock waves are regarded as a working tools.

From a wide range of available techniques, the plate impact experiments with resource to a gas gun was used to achieve the proposed results. The velocities were measured by Heterodyne Velocimetry (HetV) and for the configured setup the target was designed regarding all the shock propagation background.

The work planned herein involved using the shock impact platforms at the Institute of Shock Physics (ISP) at Imperial College of London to perform measurements of the shock wave and particle velocities in WC samples. This project builds on a collaboration between the ISP and two research units of the Mechanical Engineering Department of Coimbra, CEMUC (Centro de Engenharia Mecânica da Universidade de Coimbra) and ADAI (Associação para o Desenvolvimento da Aerodinâmica Industrial), where the WC powders were synthesized by ball milling to nominal Nickel concentrations of 11%.

1.2. Outline

The structure of the present thesis is as follows.

A modern theory of the description of shock propagation in solids and powders is presented in chapter 2. The Hugoniot relations are introduced and explained in regard to the characterization of the state of materials during the propagation of a shock wave, in terms of density, pressure, velocity of the particles and shock, among others. In fact, these relations are shown as combination of conservation equations: mass momentum and energy. The same theory is also true for powdered materials. Therefore, two different models that predict the Hugoniot relations of the material under study are presented for posterior comparison with experimental results. As a closing topic, it is included a compilation of relevant studies of shock experiments to tungsten carbides.

Chapter 3 contains the characterization of the powders Nickel-doped Tungsten carbide as well as the final state of the compacted samples. In order to compact the samples, a powder dye compactor was designed and it is described herein described.

Chapter 4 focuses on the experimental methods used for validating the whole experimental setup. A basic description of the gas gun is made, as means of providing an

understanding of its operation. Both the design of the target and the selection of the materials are featured in this chapter and are justified in a theoretical background. In regard to the adopted HetV measuring system, the basic principles of operation are explained along with the preparation, installation and usage of the setup.

Chapter 5 contains the experimental results obtained from the measuring system and the analysis of the results. The section starts with a succinct explanation of the software used for the treatment of the data. The Hugoniot curves are figured in different planes and made up of a relation between the data acquired and the conservative equations. Finally, the Hugoniot curve is compared with the results achieved by other authors, as well as Thouvenin and Mie-Grüneisen models for porous materials.

Chapter 6 summarises the key points of this thesis and addresses some considerations for future works.

2. THEORETICAL BACKGROUND

2.1. Shock waves

An impact between two similar solids moving in opposite directions with equal velocities presumes that the particles on the impacted surfaces suddenly come to a stop. This intensive impulsive loading results on a stress pulse (compressive) which moves, from the interface, in both directions along the material. Since there is no movement in the plane of impact, a uniaxial strain is generated and moves herewith the stress pulse. The shock front is the interface between the shocked and non-shocked one. The passage of the pulse along the material causes a sudden jump in pressure from P_0 to P. This change reflects on an increase of density, particle velocity and specific internal energy. Depending on the material, when subjected to a shock wave, it can has different responses like compaction, plastic deformation or even phase transition.

When a shock wave is propagating into an unstressed and at rest material, and meets a boundary, there are different possible scenarios depending on the type of interface. In the case of a free surface, when there are no restrictions on the interface and $\sigma=0$, a release wave is reflected back into the material. The velocity of the material adjacent to the surface, was found to be twice as great as the velocity of the in-situ particles – free surface approximation. On the other hand, if it is a fixed surface, it is considered that $\sigma \neq 0$ and the velocity of the particle is zero. In this situation, the wave is not only reflected but also transmitted to the adjacent material (Winter, 2009).

2.1.1. The Hugoniot relations

A clearly understanding of the propagation of shock waves can be characterized as an ideal planar shock where the propagation and the strain are treated as uniaxial – 1D. The jump between the shocked and non-shocked state is assumed as a discontinuous and adiabatic transition. Conservation of mass, momentum and energy across the discontinuity drives into the Hugoniot relationships between the specific volume ν, the pressure P, the material particular velocity u_p, the shock speed U_s and the specific internal energy e. The

equations below refers to a situation where there is no initial velocity of the impacted material (Winter,2009; Hayes, 1973). The first Hugoniot relation, equation (2.2), is obtained by applying the conservation of mass to the area *A* that is affected by the shock wave and to the balance of mass m that enters and leaves it within the time interval *Δt*.

$$\rho_0 U_s \Delta t A = \rho(U_s - u_p)\Delta t A \tag{2.1}$$

$$\rho_0 U_s = \rho(U_s - u_p) \tag{2.2}$$

The subscript 0 denotes the initial values of the material before the passage of the shock front. From the previous expression the Hugoniot density can be written as:

$$\rho = \frac{\rho_0 U_s}{(U_s - u_p)} \tag{2.3}$$

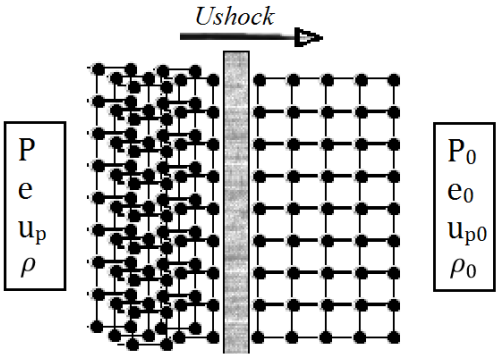

Figure 2.1. Shock wave state of material.

Due to shock there is a change of pressure during the time Δt, which can be translated in momentum and equal to an impulse. The following equation (2.5) gives the Hugoniot relation regarding conservation of the momentum.

$$(P - P_0)A\Delta t = \rho_0 A U_s \Delta t u_p \tag{2.4}$$

$$P - P_0 = \rho_0 U_s u_p \tag{2.5}$$

Before the passage of the shock wave the pressure of the material is neglected, $P_0 \approx 0$, then:

$$P = \rho_0 U_s u_p \tag{2.6}$$

Applying the principle of conservation of energy to the mass of matter within a volume $U_s\, \Delta t\, A$ it is obtained the sum of the increase of the internal energy and the kinetic energy equaling the work done by pressure acting on area *A* and moving the particles by a distance of $u_p\, \Delta t$. Thus,

$$(P - P_0)AU_s\Delta t = \frac{1}{2}\rho_0 AU_s\Delta t\, {u_p}^2 + (e - e_0)\rho_0 AU_s\Delta t \tag{2.7}$$

simplifying to:

$$(P - P_0)U_s = \frac{1}{2}\rho_0 AU_s\Delta t\, {u_p}^2 + (e - e_0)\rho_0 U_s \tag{2.8}$$

Manipulating Eqs. (2.2) and (2.5) the shock velocity U_s is obtained as well as the particle velocity u_p:

$$U_s = \nu_0\sqrt{\frac{(P - P_0)}{(\nu_0 - \nu)}} \tag{2.9}$$

$$u_p = \sqrt{(P - P_0)(\nu_0 - \nu)} \tag{2.10}$$

The positive and negative value of the solution of the square root is valid, respectively, for a compressive and for a tensile wave. The combination of Eqs. (2.9) and (2.10) into equation (2.8) results in

$$e - e_0 = \frac{1}{2}(P + P_0)(\nu_0 - \nu) \tag{2.11}$$

Equations (2.2), (2.5) and (2.11) are the Hugoniot relations justified on conservation of mass, momentum and energy, respectively. The states produced by shock compression always lie on a Hugoniot curve where the variables are continuous across planes of interaction.

Interestingly, experimental results shows that the Hugoniot of some materials can be represented by a straight line in the $U_s - U_p$ plane (McQueen *et al.*, 1970) and may be written as:

$$U_s = C_0 + su_p \tag{2.12}$$

C_0 is approximately equal to the velocity of sound

$$C_0 = \sqrt{\frac{K}{\rho_0}} \tag{2.13}$$

where, K is the bulk modulus. The slope s can be obtained for a first approximation contemplating the Mie-Grüneisen parameter, (Pruemmer *et al.*, 2006)

$$s = \frac{1}{2}(\Gamma + 1) \tag{2.14}$$

From the reference conditions of the material, Γ is: (2.15)

$$\Gamma = v\left(\frac{\partial P}{\partial e}\right)_v = \frac{v}{c_v}\left(\frac{\partial P}{\partial T}\right)_v = -\frac{v}{c_v}\left(\frac{\partial P}{\partial v}\right)_T\left(\frac{\partial v}{\partial T}\right)_P = \frac{3\alpha v}{c_v K_T}$$

where, α is the linear coefficient of thermal expansion and K_T is the isothermal compressibility.

The combination between the linear approximation of the Hugoniot (2.12) and the relations of conservation of mass (2.2) and momentum (2.5) gives the following equation that relates pressure with the specific volume.

$$P = \frac{{c_0}^2(v_0 - v)}{[v_0 - S(v_0 - v)]^2} \tag{2.16}$$

A relation between energy and thermal pressure is also given by Mie-Grüneisen equation:

$$P - P_c = \frac{\Gamma(v_c)}{v_c}(e_1 - e_c) \tag{2.17}$$

2.1.1. Hugoniot of porous materials

The Hugoniot of Powders tends to equalise the curve of dense solids but its values are always lower. In fact, the high porosity of powders leads to a dissipation of the compressive wave on a large plastic deformation, particle rearrangement against friction and particle break up, or even melting. This increase of internal energy is the explanation for the lower values of the velocity of shock waves and consequently a decrease on the slope of the function, as it seen in Figure 2.2, when comparing to solid Hugoniot.

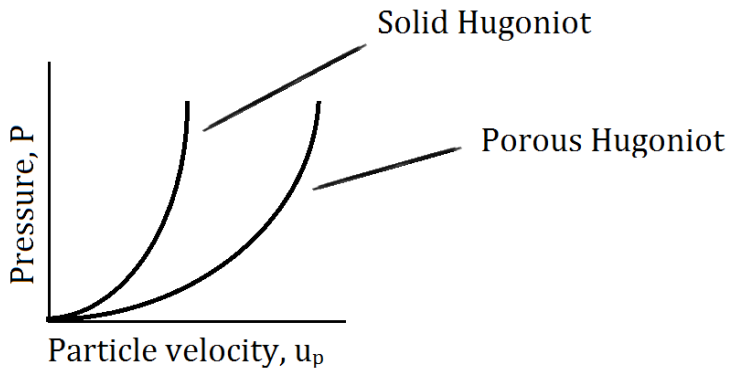

Figure 2.2. The Hugoniot curve of solid and porous materials in the P – u_p plane.

2.1.1.1. Mie Grüneisen Model

The Mie-Grüneisen equation for obtaining the curve resorts to the curve of the respective solid material. This model founds in an equilibrium state in the non-shocked material. If the relation (2.17) is written for a porous and a solid material, and if the equation can be equalised by the parameter e_c then,

$$e_{p1} - e_{s1} + \frac{\nu_{s1}}{\Gamma(\nu_{s1})}(P_{s1} - P_c) = \frac{\nu_{p1}}{\Gamma(\nu_{p1})}(P_{p1} - P_c) \tag{2.18}$$

The subscripts *s* and *p* refers to the porous material and the corresponding solid respectively.

When $\nu_{s1} = \nu_{p1} = \nu_1$the previous equation results,

$$e_{p1} - e_{s1} = \frac{\nu_1}{\Gamma}(P_{p1} - P_{s1}) \tag{2.19}$$

Rewriting equation (2.11) for the two cases, porous and solid materials considering that P_0 is negligible when compared with the pressure of the shock:

$$e_{s1} - e_{s0} = \frac{P_{s1}}{2}(\nu_{s0} - \nu_{s1}) \tag{2.20}$$

$$e_{p0} - e_{p1} = \frac{P_{p1}}{2}(\nu_{p0} - \nu_{p1}) \tag{2.21}$$

Equating them into (2.19)

$$e_{p0} + \frac{P_{p1}}{2}(\nu_{p0} - \nu_{p1}) - e_{s0} - \frac{P_{s1}}{2}(\nu_{s0} - \nu_{s1}) = \frac{\nu_1}{\Gamma}(P_{p1} - P_{s1}) \tag{2.22}$$

Previous experiments performed by other authors revealed that the initial internal energy of powdered and solid materials is similar, then the following equation is function of the pressure and specific volume of the material.

$$P_{p1} = \frac{P_{s1}\left[\frac{\Gamma(\nu_{s0} - \nu_{s1})}{2\nu_1} - 1\right]}{\left[1 - \frac{\Gamma(\nu_{p0} - \nu_1)}{2\nu_1}\right]} \tag{2.23}$$

Lastly, the following equation allows to estimate the Hugoniot curve of the powder material if the parameters S and C of the Hugoniot curve of the solid are well known likewise the initial specific volume of both states of the material. (Ribeiro 2003 and Herrmann, 1969)

$$P_{p1} = \frac{[2\nu_1 - \Gamma(\nu_{s0} - \nu_1)]c^2(\nu_{s0} - \nu_1)}{[2\nu_1 - \Gamma(\nu_{p0} - \nu_1)][\nu_{s0} - S(\nu_{s0} - \nu_1)]^2} \tag{2.24}$$

The Grüneisen parameter Γ is approximately constant whenever the specific volume changes are small. However, if it is the case of studying the behaviour of the materials when there is a high change of pressure and consequently significant change of specific volume, the coefficient between Γ and ν is considered constant.

$$\frac{\Gamma(v)}{v} = \frac{\Gamma(v_0)}{v_0} = const. \tag{2.25}$$

2.1.1.2. Thouvenin Model

In 1965, Jacques Thouvenin came up with a theory which he nominated as Thouvenin Model or Plate Gap Model. (Thouvenin, 1965). Differently from other authors, Thouvenin's founded his model in the way how a wave propagates in a material instead of the thermodynamic nature. The porous solid material is seen as an assembly of solid plane plates with equal thickness *a*, separate by a distance of *b*, therefore the specific mass of the set is equal to the specific mass of the porous solid in analysis. Schemed on Figure 2.3, the propagation of the waves came from the successive impact of the different plates, that results on the creation of the shock waves and its expansion. The model considers the propagation of the wave as unidimensional.

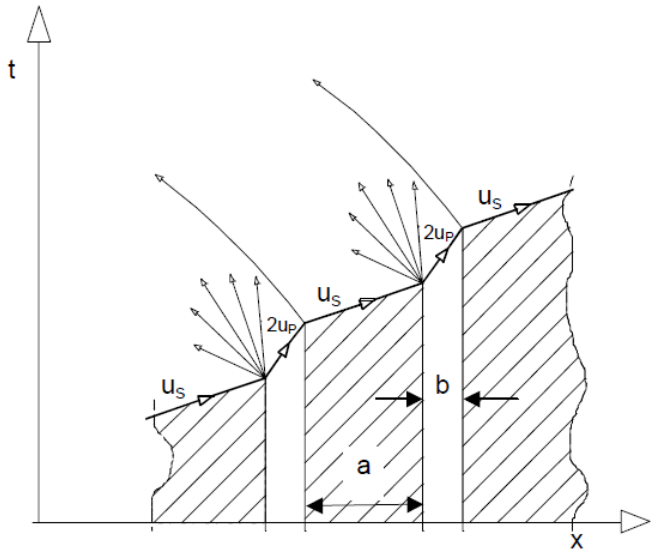

Figure 2.3. Schematic representation of the model of Thouvenin (Thouvenin, 1965).

When a shock wave with a velocity of U_s propagates into the first plate and meets its backing interface, it acquires a velocity of $2\,u_p$- free surface approximation. On that instant, expansion waves are created with opposite direction to the movement, reducing the pressure to zero. The impact of the first plate on the second one, results in a shock wave that

propagates with a velocity of U_s in the plate in rest. On the other hand, on the impacting plate the wave propagates with a velocity of $U_s - 2u_p$. The same process is repeated on the remainder plates, and in the global, not only a single shock is generated but a periodic series of shock in the plates and projection of matter for the space between the plates. (Ribeiro and Campos, 2003)

The sequence of impacts propagates with a velocity u_{sp} and its meaning cannot be misunderstood neither confound with the velocity of the shock. According with Thouvenin, before relating these parameters with the conservation equations it is necessary to make some modifications.

A parameter λ is introduced as inverse of the porosity α

$$\lambda = \frac{1}{\alpha} = \frac{Specific\ mass\ of\ the\ porous\ solid}{Specific\ mass\ of\ the\ non-porous\ solid} = \frac{a}{a+b} \tag{2.26}$$

The parameters *a* and *b* of the previous equation are represented in Figure 2.3. The relation between the time span of the propagation of the shock on the plates and the movement of the free surface within the gap *b* is written as:

$$\frac{1}{U_{sp}} = \frac{\lambda}{U_{ss}} + \frac{1-\lambda}{2.u_{ps}} \tag{2.27}$$

$$\frac{1}{u_{pp}} = \frac{\lambda}{u_{ps}} + \frac{1-\lambda}{2.u_{ps}} \tag{2.28}$$

Equations (2.27) and (2.28) allow to calculate the velocity of shock and the particle velocity. Although it was not completely in accordance with Thouvenin statements, Hofmann *et al.* (1968) defended that the relation between *P* and ν could be deduced by relating the conservation equations and u_{sp} and u_{pp} .

2.1.2. Tungsten Carbide shock data

Properties of the shock waves of tungsten carbides have been studied throughout the past years. McQueen *et al.* (1970) studied the shock Hugoniot of near full-density tungsten carbide with 5wt% Co. In 1995 and 1999 Grady reported shock data of two types of WC materials. The first one, produced by Kennametal Company, contained 5.7wt% Co, 1.9wt% Ta along with less than 0.9wt% Nb and Ti while the second material, extracted from armor piercing (AP) rounds, contained 3–4wt% Ni, 0.4-0.8wt% Fe and 0.05-0.2wt% Co. Amulele *et al.* (2008) made tests to a material produced by Cercom, a ceramic with 97.2wt%

WC and 228wt% W_2C. All the materials had a density within 14910 and 15700 kg/m^3. In Figure 2.4 is plotted the shock data for the referred tungsten carbide ceramics.

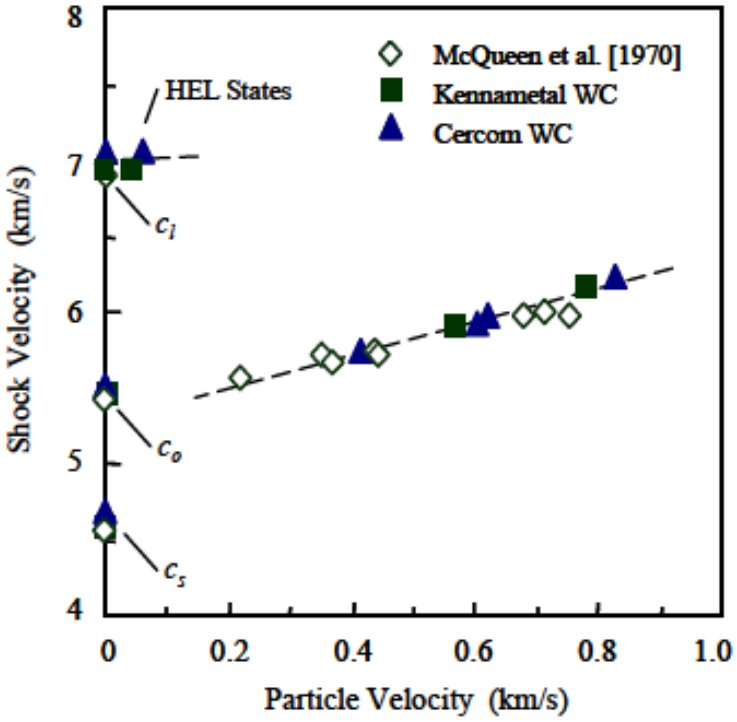

Figure 2.4. Experimental shock velocity versus particle velocity (Grady, 2009).

Vogler *et al.* (2005) performed plate impact experiments to determine the Hugoniot properties of WC powders. Once again WC was manufactured by Kennametal, with a purity of almost 100%. A single stage gas gun was used to achieve shots at an impact velocity of 245, 500 and 711 m/s. Vogler and collaborators measured the shock velocity by matching impedance technique and plotted the graphic U_s-u_p represented in Figure 2.5.

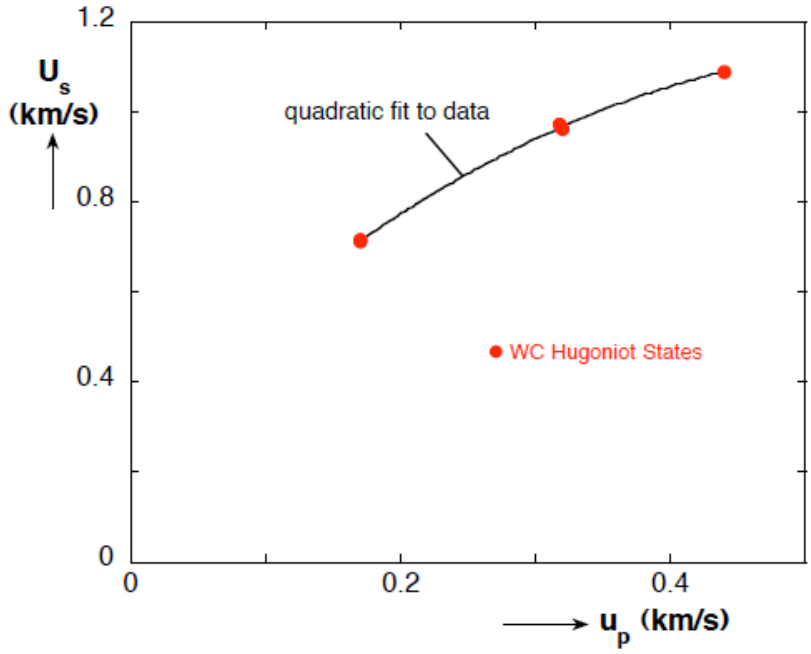

Figure 2.5. Measured shock velocity for WC powder versus in-material particle velocity determined though impedance matching techniques (Vogler *et al.,* 2005).

3. MATERIALS AND METHODS

3.1. Tungsten Carbide, WC

Tungsten carbide, a cemented carbide which is also designated as a hard metal, is commonly used for applications that require high levels of hardness and wear resistance. Thus, its excellent properties make of it a useful material in the production of cutting tools and molds, among other applications. The first development of WC took place in Germany, in the early 20's, by Osram, an electrical lighting company that sought an alternative to diamonds for machinating metals. Later, in 1925, a license was sold to Krupps and in 1926 this company launched to the market sintered carbide tungsten named as WIDIA, an acronym for Wie Diamant - like diamond (at ThyssenKrupp's website).

3.1.1. Tungsten carbide powders

The WC powders used in the present study were produced by DURIT - Metalurgia do Tungsténio, Lda. and its general characteristics are summarised in the following Table 3.1.

Table 3.1. Characteristics of GD20N powders (Pires, 2012).

	Ni [wt%]	**Theoretical density [g/cm^3]**	**Specific volume [cm^3/g]**	**d_{50} [µm]**
GD20N	11	14.7	0.068	1.2

Differently from what the literature states, WC was mixed with Nickel. This element has been on the focus of some researchers insofar as an adding material in WC, because the mechanical properties achieved in WC-Ni are very similar to the popular WC-Co, conceding better resistance to corrosion and higher values of hardness. These adding materials, also called as soft materials of the mixture, have been used in WC to facilitate the compaction of the powder and its final form. Its excellent characteristics results from the combination of properties granted by the presence of two different phases where WC phase

imparts the hardness and strength whilst Ni matrix acts to increase plasticity and toughness (Shon *et al.*, 2007).

3.1.2. Powder characterization

According to Pires (2012) the powders were characterized by SEM (Scanning Electron Microscope) and XRD (X-Ray Diffraction). The observation of SEM results indicates that WC particles have an irregular shape and size distribution between 0.3 and 3 μm without cleavage edges along the counter. The bigger size of WC distinguishes it from the Ni in the GD20N powders. The structural characterization, made by XRD, demonstrated two compounds on WC powder, whose principal phase is WC and tungsten semi-carbide the secondary one, both with hexagonal structure. GD20N revealed the same constitution plus Ni with a cubic structure.

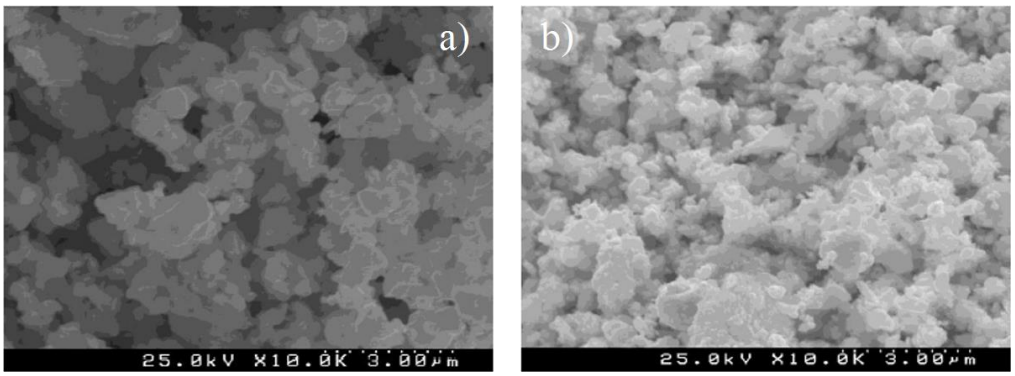

Figure 3.1. Morphology of Powder: a) WC and b) GD20N (Pires, 2012).

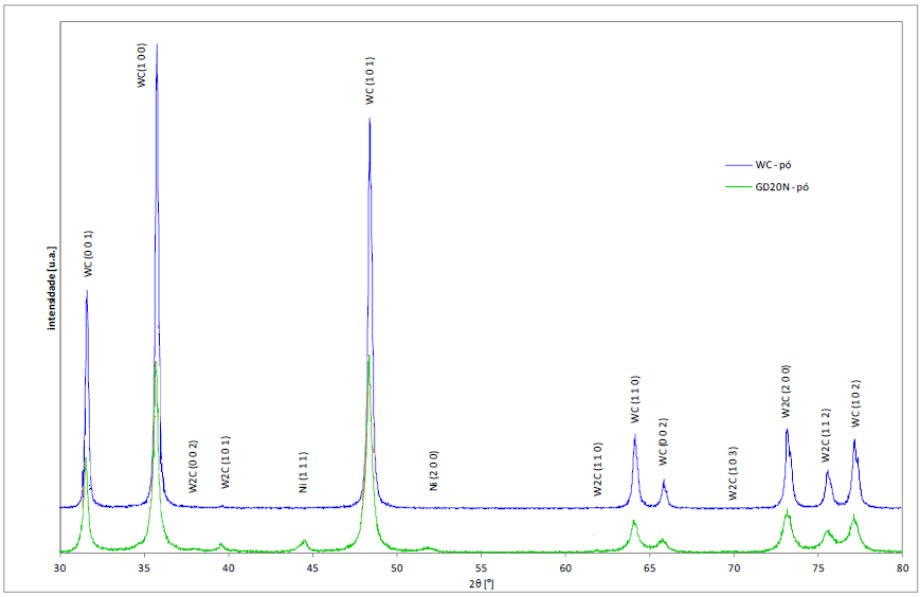

Figure 3.2. X-Ray Difractogram of WC and GD20N powders (Pires, 2012).

3.2. Powder compaction

For the purpose of comparing the results achieved, it is presupposed that the powder samples are geometrically similar and prepared within the same conditions. Although the rings are 3mm height, the compressed powder must have 1mm height to better control the shock wave interferences. To fulfil these initial conditions, primary calculations on the amount of powder for each material were necessary and were based on the densities calculated by DURIT. For the right amount of powder, 5% was added, accounting for predictable losses, such as powder that typically gets stuck in the cavity of the dye and in the interior surface of the ring. A force of 8 kN was applied to the punch of the dye.

3.2.1. Isostatic pressing dye

In order to compress the powders into a certain density, an isostatic compressing dye was designed. This device was made in hardness steel and was manufactured with very low tolerances to achieve a precise geometry, good finishing of surface and a uniform density of the specimens.

Figure 3.3 presents all the separate pieces of the compactor. The body, divided in two pieces, is connected by the two aligning pins and four screws. The inner surface of the body has a principal cavity that allows a fit sliding of the punch, and a secondary hollow that holds the ring along with the bottom base. It is common on this kind of procedures that

the sample gets damaged while it is collected from the device. However its opening geometry was specially designed to avoid deterioration by infiltrated powder between cavity's interface and the ring. Also showed in the figure bellow, is the confining ring, made in steel with 7.5mm of diameter and 3mm of height.

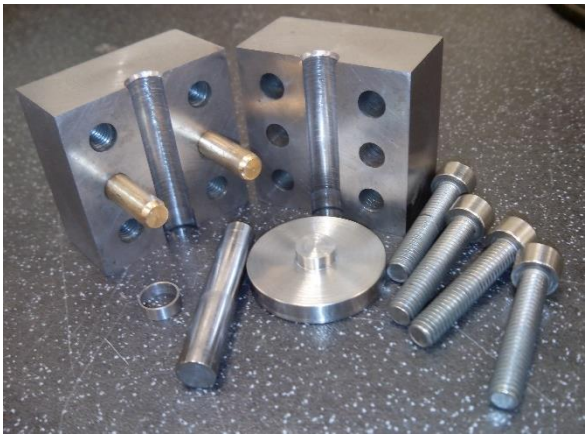

Figure 3.3. Isostatic compressing dye and ring.

3.2.2. Density measurement

The relative density of the compacted (green) samples was determined by the relation of the density of the powders and its theoretical values. The densities were calculated using the relation mass-volume (3.1) and values are provided in Table 3.2.

$$\rho = \frac{m}{h\pi \frac{d^2}{4}} \tag{3.1}$$

Table 3.2. Density measurements of the samples.

Specimen number	Mass [g]	Thickness [cm]	Density [g/cm^3]	Specific volume [cm^3/g]	Theoretical values of density [g/cm^3]	Relative density [%]
#25	0.395	0.1149	7.777	0.129	14.7	52.9
#27	0.319	0.0865	8.349	0.120		56.8
#31	0.419	0.0963	9.839	0.102		66.5

All the rings of the sample were measured and weighted for a final ponderation of the density. Sample *#31* has a density of 66.5%, a higher value than the other specimens. It is thought that the reason for this difference between values is due to the equipment used for pressing the dye punch. For logistics reasons, it was applied a different equipment on sample *#31*.

4. EXPERIMENTAL METHODOLOGY

4.1. Gun description

Housed in the Laboratory of Shock Physics at ICL, a single stage gas gun with a 13mm bore, showed in Figure 4.1, was used to conduct plate impact experiments. A gas gun makes use of compressed gas filled into a reservoir behind the projectile to accelerate it. Helium was the chosen gas owing to its low molecular weight. Depending on the desired velocity to the projectile, the gas is pressurised into a certain value and when the "fire" button is pressed, an electronically signal is given to a super-fast valve that releases the gas which drives the sabot down the 3 meters barrel. The impacted area is confined by a vacuum chamber connected to the barrel and also to an empty air tank (also subjected to vacuum). This experiments are performed in vacuum conditions due to safety measures and better accuracy on the results. Variables like temperature and pressure became more stable and do not interact with shock waves. Regarding safety problems, it is known that high values of pressured air is released, and even that the chamber is sealed, all the system can explode by overpressure. On the other hand if there is no air, the shock waves cannot propagate and extinguish.

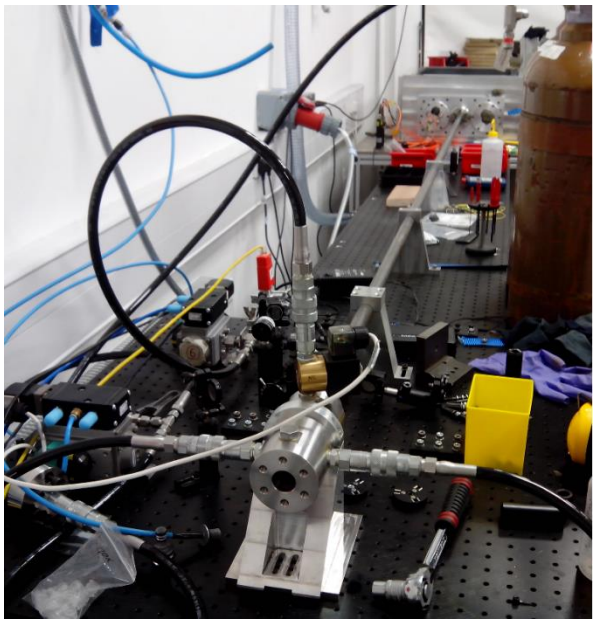

Figure 4.1. Gas gun at ISP laboratory.

4.2. Target configuration

The element that is impacted by the projectile is the target. It was especially designed for studying the velocity of the shock waves for this 13 mm bore gas gun. A total of four pieces can be described on this target setup: a cooper plate, a sample holder, an optical fibre holder and the sample.

4.2.1. Target setup

In the moment of the impact, the sabot collides with a cooper plate placed on the forward surface of samples. A thickness of the samples of approximately 0,70mm were thought to avoid border interferences – reflected waves from the counters of the material. Knowing that impurities on the material create diffraction of the wave, oxygen free high conductivity cooper with a purity of 99.99% was peculiarly chosen as a material of interest. To guarantee planar surfaces without defects, both faces were lapped on the lapping machine.

Along with cooper, the sample and optical fibres holders restrain the specimen. The PMMA holders were cut by laser with very low tolerances. The first piece has a cavity where the ring with the powder fits perfectly. Right around that area, there is a special contour without material that allows the sensors to measure the velocity of the free surface of the cooper. Projected to align the fibres, one on the centre and three equally distanced from it and themselves, the fibre holder also pressurises the sample against the cooper.

This setup is mounted on the mounting set that is constituted by an adjustment bracket and the target holder. In order to allow an easy displacement of the two parts of the target, they are connected by plastic screws. On the lateral of the holder, there are two holes that allow the beams of the light gates to pass through it, to measure the velocity of the impactor. The following figure pictures and describes the entire target configuration.

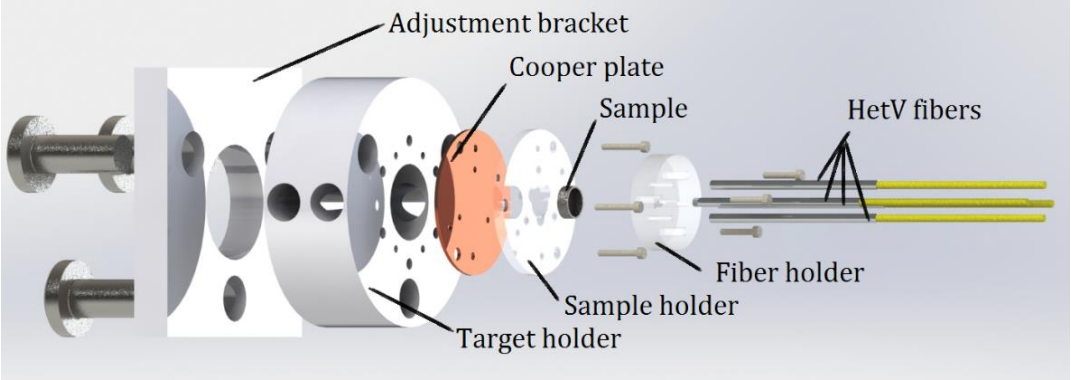

Figure 4.2. Target configuration and description.

4.2.1.1. Reflective back surface

As it will be referred in section 4.4, interferometry was the adopted measurement technique and it requires that the moving object has a reflective back surface, so that there is enough signal on the oscilloscope. After the first shot (experiment I) it was noticed that the signal for lower velocities could not be enough for a clean data, therefore a 25µm sheet of brass was applied on the back surface of sample *#27* (experiment II) to guarantee a good reflection of the laser. It is important to notice that depending on the material chosen for the reflective window, a very small inaccuracy on time and velocity can be added to the measurements.

4.2.1.2. Alignment of the target using two laser setups

Inside the vacuum chamber the target must be hold in the most precise position, as a misalignment may implicate critical errors. To prevent these sort of inaccuracies, it is essential to align the centre of the sabot with the centre of the target (impacted area) and the parallelism between the shocking areas, in order to avoid interferences stemming from the tilt. It is possible to fulfil these conditions by using two laser setups.

It is important to notice that the equipment used for the alignment should be very precise and that any change on temperature can be reflected on a displacement of the adjusting micrometric screws. Hence, the alignment must be made right before each experiment so as to avoid errors. This alignment should mitigate any effects of the project tilting, resulting in a normal impact.

There is a direct relation between the error on this technique and the diameter of the beam. An easy calculation using Pythagorean Theorem relating the length of the beam

and its diameter gives the imprecision in degrees. For a 3m barrel and 0.001m of the diameter of beam, the maximum misalignment is approximately 0.33 x 10^{-3} degrees.

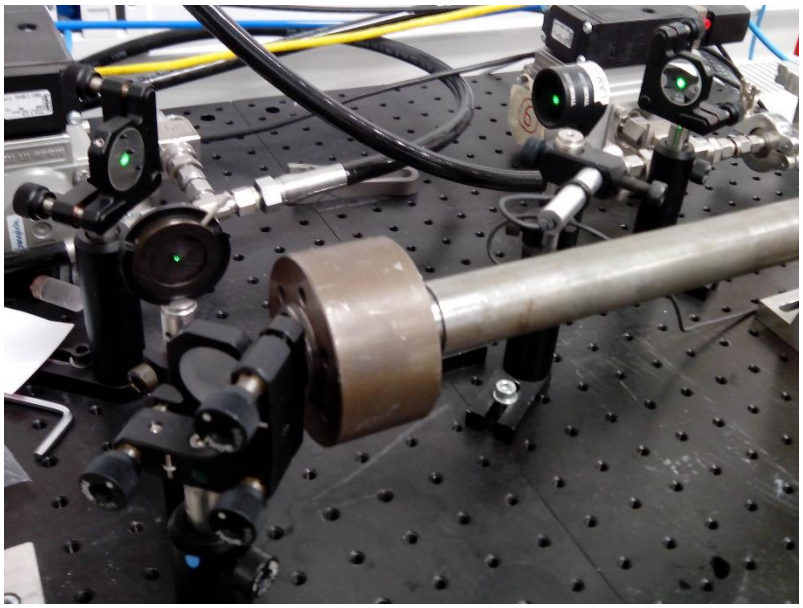

Figure 4.3. Alignment the centre of the shocking areas.

4.2.1.2.1. Alignment of the mirror of reference

All the midpoints of the equipment must be at the same height of the centre of the barrel, particularly the iris since it will be considered the reference. As it is shown in Figure 4.3, the mirrors are positioned in a triangle rectangle geometry, with the third mirror aligned with the barrel. The source must point to the centre of the first mirror that adjusts the height of the beam and the parallelism with the board. For safety measures, it is necessary to set a filter between the first two mirrors to reduce the intensity of the beam. The second mirror rectifies the perfect alignment and the parallelism of the beam by comparing two positions with the iris. Once the beam intersects the region of the iris, the following step is adjusting the last mirror so that the beam goes through the barrel to the vacuum chamber and, in a vertical and perpendicular surface, designs a pattern of concentric circles. Thus, the correct position for the centre of the target was achieved. It is important to notice that if the laser is not well positioned in the first steps, the pattern is difficult to obtain, due to reflections on the interior of the barrel (mirror finish).

The mirror of reference must be placed in manner that it is perpendicular to the laser beam, to reflect it in the opposite direction. This alignment can be noticed by concentric

circles around the surface of the iris. This pattern is the result of the diffraction of light after the first passage on the iris.

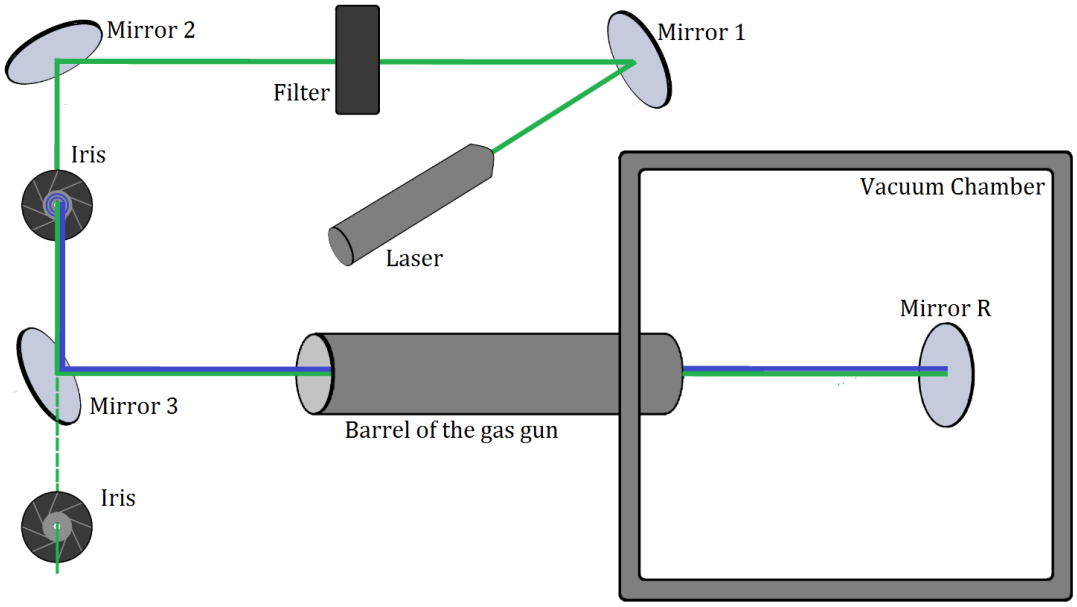

Figure 4.4. Laser setup for alignment of the mirror of reference.

4.2.1.2.2. Alignment of the target holder

The first part of the target holder is aligned with the sleeve that goes inside the barrel and fits on the holder. A red laser set, as schematised on Figure 4.5 is used to align the perpendicularity of the second mounting. A mirror must be set on the surface of the mounting. Similar to the previous alignment, the concentric circles pattern has to be seen on the iris. Once the mirror R was previously aligned, it is only necessary to adjust the target holder.

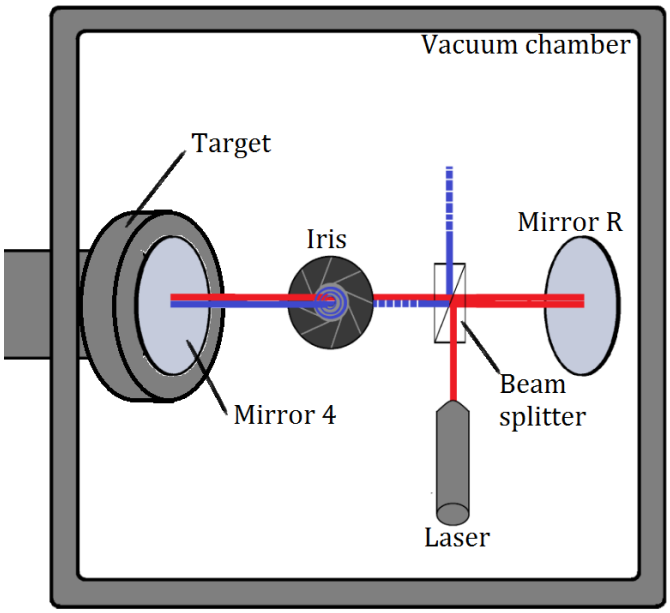

Figure 4.5. Laser setup for alignment of the target holder.

4.3. Sabot configuration

The projectile, also named impactor, flyer or sabot, is made of a very light weight PMMA (Poly Methyl Methacrylate) and oxygen free high conductivity cooper. This type of cooper, also used on the impacting surface of the target, while impacting, creates a steady shock wave on the material. The sabot also wears two sealing rings that along with its design, seals the launch tube maximising the efficiency of the acceleration by the gas.

According to the velocity of the impact, two different sabots were used. The first one, for lower velocities, has a dense solid body with a 2mm copper. For velocities greater than 550m/s was used a lighter sabot with a hollowed PMMA body and a 1mm cooper disk. Figure 4.6 shows the high velocity sabot, although both of them have a similar geometry.

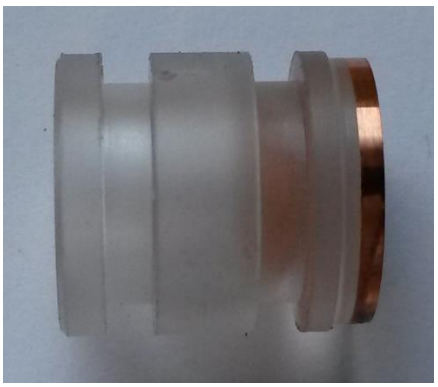

Figure 4.6. High velocity sabot.

4.3.1. Velocity of the sabot

A set of two light gates and an oscilloscope was used for measuring the velocity of the sabot. Referred in 4.2.1, the target holder had two holes on the lateral surface which allowed the passage of two laser beams distanced by 11.211mm. When the laser beams would be interrupted, start and stop signal, on the oscilloscope was generated a temporal data. Distance and span of time led to the velocity of the sabot. Figure 4.8 a) and Figure 4.9 picture the basic setup.

4.4. Heterodyne velocimetry

The most common techniques for measuring velocities up to several kilometres-per-second are VISAR system, Fabry-Perot-based system and Heterodyne Velocimetry (HetV), all based in interferometry. This last technique provides a point of an interface velocity with high temporal resolution resorting to many products developed for the communication industry, such as fibre laser and single mode fibres.

4.4.1. Basic principles of operation

A HetV setup is schematically represented in Figure 4.7, where the different components and the path of the light are distinguished. A light with a frequency f_0 is launched from a laser through the optical fibre, which in its end can have a lens responsible for emitting the light and collecting part of it that is reflected or scattered by the moving surface. Because it has to reflect an amount of light sufficient to guarantee reliable data, the surface of study of the specimen must retain a reflecting finish. The collected Doppler-shifted light, f_d (reflected light), is transported by fibre to the detector and is mixed to a portion of the emitted light with frequency f_0, which is sent directly from the laser (Strand *et al.*, 2004).

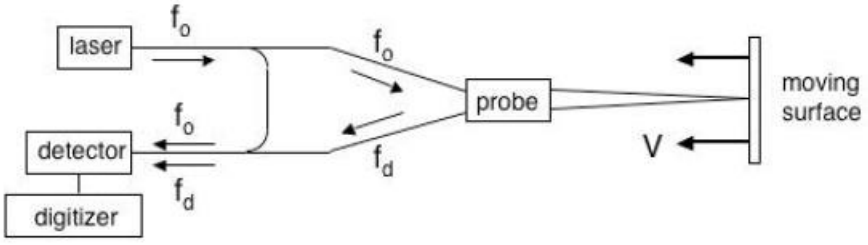

Figure 4.7. Schematic representation of HetV (Strand *et al.,* 2004).

The detector generates a beat frequency f_b proportional to the velocity:

$$f_b = f_d - f_0 = 2(v/c)\, f_0 \tag{4.1}$$

With a speed of light c:

$$c = f_0\, \lambda_0 \tag{4.2}$$

where λ_0 is the wavelength emitted by the laser.

Determined f_b and λ_0, the velocity v is given by:

$$v = \left(\frac{\lambda_0}{2}\right) f_b \tag{4.3}$$

In plate impact experiments $f_d > f_0$ inasmuch as the surface is moving toward the probe.

4.4.2. Measuring technique

As referred in section 2.1.1, Hugoniot parameters can be described if at least 2 variables are characterised. The experimental setup was designed to measure the particle velocity and the velocity of the shock wave. The high level of precision for experimentally determining these parameters, required meticulous alignments and measurements. All the procedures followed certain rules and were adapted in function of the equipment available on ISP laboratory.

Heterodyne velocimetry allows to measure velocities of flying objects using interferometry technique. Thus, the particle velocity was directly measured with this technique while the velocity of the shock waves was derived from the distance travelled by the waves within a span time. Figure 4.9 schematised the whole measuring setup and Figure 4.8 depicts the HetV setup and identifies each sensor.

4.4.2.1. Velocity of the free surface of the sample

Each set of the target has four sensors for measuring velocity and time. The first parameter, particle velocity, is obtained by C1, the central sensor that picks up the velocity of the free surface of the back surface of the compacted sample. The centre of the sample was chosen as region of interest to avoid border interferences.

4.4.2.2. Velocity of the shock wave

Calculating the velocity of the shock wave is more complex than the previous parameter. At the moment of impact, the wave is created in both impacting surfaces (the

target cooper and cooper flyer interfaces). Regarding the target side, the shock propagates along the cooper until the interface with the powder. As soon as the shock front arrives the back interface of the cooper, it arrives to the powder, therefore, that instant of time is acquired by C2, C3 and C4. Ideally the instants of time would be exactly the same but due to uncontrollable errors, the sabot impacts with a small tilt that generates different arriving instants of time. The mean time of the measured values gives the instant of time when the shock wave was transmitted to the powder while C1 reads the value of the arrival of the shock to the back surface of the powder. The difference between this two values is the span time that the wave travelled along the compacted powder. Using the basic equation (4.4) , the velocity of the shock wave can be calculated.

$$U_{shock} = \frac{x_{sample}}{\Delta t} \tag{4.4}$$

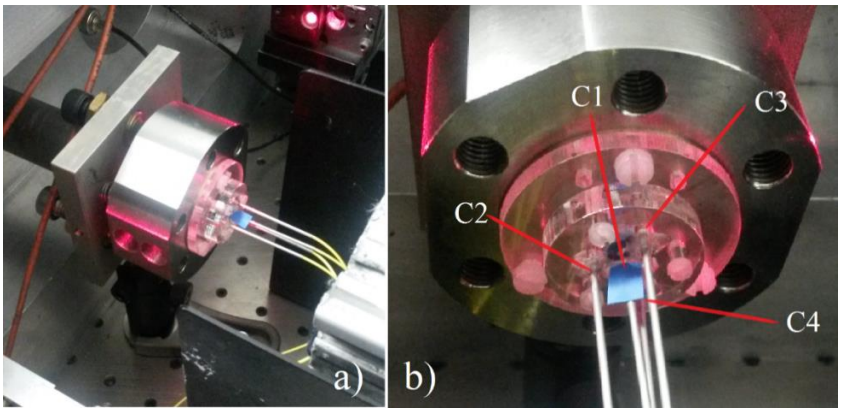

Figure 4.8. a)HetV sensors setup and light gates; b) HetV sensors setup identification.

4.4.3. Setup

The setup used on this experiment is schemed in Figure 4.9. The light is transported to the experiment via single mode fibres-optic (1550nm), which are connected to the channels on the combo box, an assembly of a fibre laser, a detector and an amplifier. An oscilloscope Lecroy WaveMaster 816 ZI-A, with a bandwidth of 16GHz, 4 input channels and 40GS/s max sample rate converted the signal into a beat frequency. The channels of this device are connected to the specific channels of the combo box (represented in blue on the figure below). At the appropriate time, a trigger signal is to be sent to the oscilloscope from the system that measures the velocity of the sabot. When the projectile interrupts the second trigger of the system that measures its velocity, a trigger signal is sent

to the HetV system oscilloscope to start digitising (connection between oscilloscopes is represented in green on the figure below).

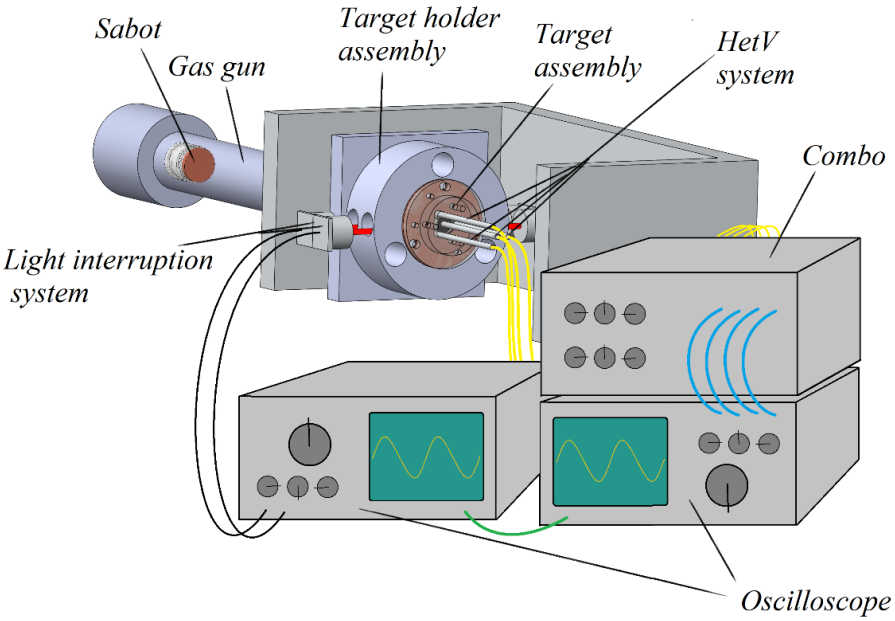

Figure 4.9. Gas gun, target assembly and measuring systems setup.

4.4.4. Preparation of the optical fibre

HetV setup demands four optical fibres for each shot. The fibres were carefully prepared using a non-consensual technique created for the desired experiments, which allowed using single mode fibre-optic that were previously damaged in experiments.

Before implementing the technique, all the chosen fibres were tested with a portable laser and a fibre microscope, to guarantee that the lens were not damaged. Primarily, to avoid contaminating the lens, all the four-set fibre were placed on the fibre holder with the metallic tube on it. All the fibres were cut with a length of 90 cm and stripped 5 cm. The following step was cutting the core 3 cm, using a high precision cleaver, to guarantee an exact cut, without breaking the optical glass. After this, 2mm of the clad was stripped and dragged out until right before the tip of the core (≈1mm of distance).

In order to protect the fibre, the protective metallic tube was glued into it, guaranteeing a distance of approximately 0.5 mm to the tip of the fibre. Figure 4.10 is a scheme of the fibre showing off a section view from the tube. On the target assembly, the fibres were glued to the fibre-holder with a distance from the powder and the cooper of approximately 0.5 mm.

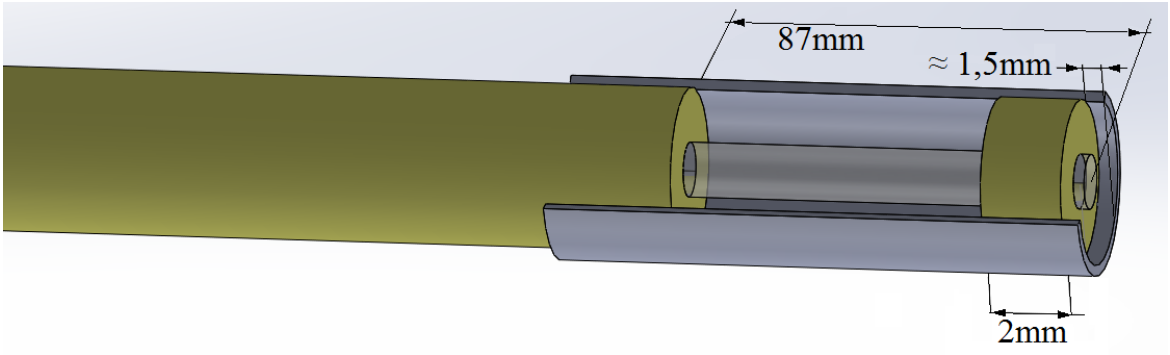

Figure 4.10. Schematic section view of optical fibre.

4.4.5. HetV system calibration

A measuring system always requires previous calibration for precise and exact measurements. Before the experimental shots of reference, one shot was performed for calibrating the system and also adjusting the laser output for the desired power levels at the detectors.

Each HetV setup is connected to distinct channels on the oscilloscope. Although the assembly for each channel is similar, the calibration of the response of the system must be done to achieve accurate input values. In order to find the correct time discrepancy between the channels, a simultaneous input signal must be created to make the relative error correction with a single measurement by using a beam splitter. The input signal is created performing one shot for test. A single-probe beam is split into four beams of equal intensity and connected on each channel. The data was analysed and manipulated. Channel C1 was made the reference for the time correction, and Figure 4.11 shows the calibrated data and the corrective time for each channel: C1 (0μs); C2 (0.001 μs); C3 (-0.006 μs); C4 (+0.005 μs).

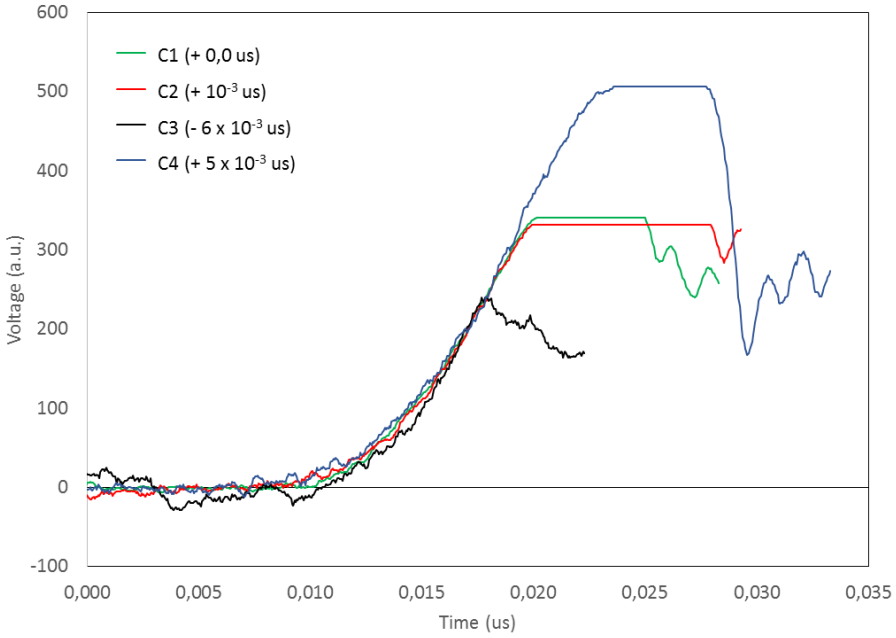

Figure 4.11. HetV curves of calibration shifted in time to overlay.

5. RESULTS AND DISCUSSION

The principal objective of this work is to determine the Hugoniot relation of the GD20N powders prepared for these experiments. For this effect, the previously described gas gun setup was used.

A total of five plate impact experiments were performed, but only three were conducted to Hugoniot data. The remaining two shots were performed with the purpose of calibrating the HetV and checking the alignment. Summarised in Table 5.1, is the characterisation of the conditions previous to the impact on the target

Table 5.1. Characterization of the experimental shots.

Shot	Sample/ mass [g]/ thickness [mm]/ Brass [mm]	Sabot/ m_{sabot} [g]	Cooper plate thickness/ tol/tol [mm]	Light gates time [µs]	Light gates distance [mm]	Velocity of the impactor [m/s]
I	#25/ 0.395/ 1.149/ -	2mm Cu/ 6.08	0.690/ +0/ +0	22.5	11.211	498.2 ≈500
II	#27/ 0.319/ 0.963/ 0.025	2mm Cu/ 6.05	0.694/ +0/ +0	35		320.3 ≈320
III	#31/ 0.419/ 0.963/ -	1mm Cu/ 2.48	0.691/ +0/ +0	17		659.5 ≈660

On shot II it was used a sample with a 25 µm brass reflective back surface which, on the analysis, the window will be neglected because its thickness is very low and due to its high impedance, the material gains the velocity of the free surface of the powder. As

referred in 4.3, for high velocities, the sabot considered must be different. Hence on experience III the 1mm Cu sabot was used.

With a distance of 11.211 mm between the light gates, the velocity of the sabot was calculated regarding the time counted on the oscilloscope. Three points between C2, C3 and C4 were measured to check an equal thickness on that area (represented as a cross in Figure 5.1)

Figure 5.1. Cooper target and reference points of measurement of the thickness (represented as a cross).

5.1. Data analysis

The data collected from the HetV measurements was analysed with resource to the software HetV Analysis Tool version 2.08. On this type of measurements the variables of interest are frequency and time. This data is obtained by using a sliding Fourier transform (FT) on a time-varying sinusoid.

The software runs a code that performs several preparatory operations on the beat wave form prior to perform the actual FT. First, the user must input the start and finish time for analysis and define a window – desired number of points which the FT should be performed (Strand *et al.*, 2004). The window function called *Hamming* is chosen to reduce the undesirable effects related to the spectral leakage. Therefore, it reduces the side lobe leakage causing the main lobe to broaden or in another words, reducing the resolution (Kumar *et al.*, 2011). Given these inputs to the software, the sliding Fourier transformer is calculated and displays an image of frequency in function of time.

For the present case, it is important to analyse the instant of time when the wave arrives the surface of interest and its velocity. As it is seen in Figure 5.2, the mark on the curve represents the considered instant of time, the passage from an elastic precursor to the plastic wave: sinusoidal wave. On the graphic velocity *vs.* time, once there is a lot of noise

on the region of interest, it is necessary to make an interpolation within a drawing polygon – ROI. Constraining this area for analysis, allows to discard unwanted noise in the frequency spectrum and in the final velocity history. Attention must be taken while choosing very short windows in the hope of obtaining very high time response. However, if the length of the window is small enough to approach the size of a single beat, the code will return noisier data with increased errors of velocities.

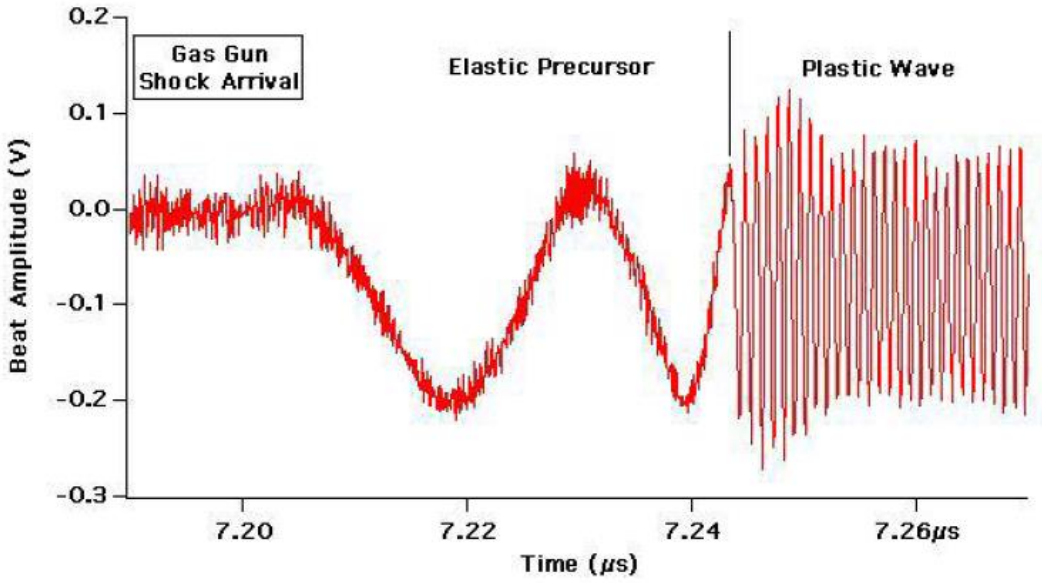

Figure 5.2. Elastic and Plastic wave on Amplitude vs. Time graphic (Strand et al., 2004).

5.2. HetV results

Three experiments were performed on GD20N powder at nominal velocities of 320, 500 and 660 m/s. The results which consist of interface particle velocity measurements and calculated shock velocities are displayed in this section. All the following figures, graphics time-signal and time- velocity are shifted on time as it was explained in chapter 4.4.5. In general, the data of the velocity of the free surface of the powder was analysed according to the following window parameters: Hamming - 512; Overlap - 409 and FFT - 4096. Different colour filters were applied to the graphics for better resolution.

Table 5.2. HetV data.

Shot	Sample GD20N	HetV sensor	$u_{free\ surface}$ [m/s]	Instant of time [μs]	Mean time [μs]	Tf-ti [μs]	U_{shock} [m/s]
I	#25	C1	520 ±15	11.7950 ±0.002	11.7950	0.9577	1199.75
		C2	-	10.8040 ±0.001	10.7923		
		C3	-	10.8669 ±0.001			
		C4	-	10.7060 ±0.001			
II	#27	C1	303 ±7.5	16.2820 ±0.006	16.2820	0.9985	866.34
		C2	-	15.3720 ±0.002	15.2836		
		C3	-	undefined			
		C4	-	15.1951 ±0.001			
III	#31	C1	602 ±7.5	14.2154 ±0.002	14.2154	0.5949	1637.34
		C2	-	13.8596 ±0.001	13.6205		
		C3	-	13.3713 ±0.001			
		C4	-	13.6307 ±0.001			

5.2.1. Experiment I, impact at 500 m/s

One experiment was conducted at 498.2 m/s, approximately 500 m/s. The plot signals of all the sensors can be seen in Figure 5.3. The first graphic of the figure shows the intensity of the signal on C1. It was registered some interference on the data, so 4ns were given for tolerance. On the remaining figures, the arrival of the plastic wave is obvious, though there is an inaccuracy of 2ns. The time of the propagation of the wave in the powder was about 0.9577 µs, which, considering 1.149mm of thickness, accounts for a velocity of 1199.75 m/s.

The velocity of the free surface of the powder is taken from Figure 5.4. This analysis took a considerable amount of time, as there was significant interference, which added to the fact that data was not so intuitive. The window parameter overlap was then changed to 150, which resulted in lower resolution, but clearer data. On the plot signal graphic, it was perceived the moment when the wave arrived at the sensor and, taking that value as a reference, it was observed on the spectrogram which data might be used. After selecting such information, the values were interpolated on the region of interest to better figure out the velocity. It was estimated that the value would be of approximately 520 m/s, with a maximum error of 30 m/s.

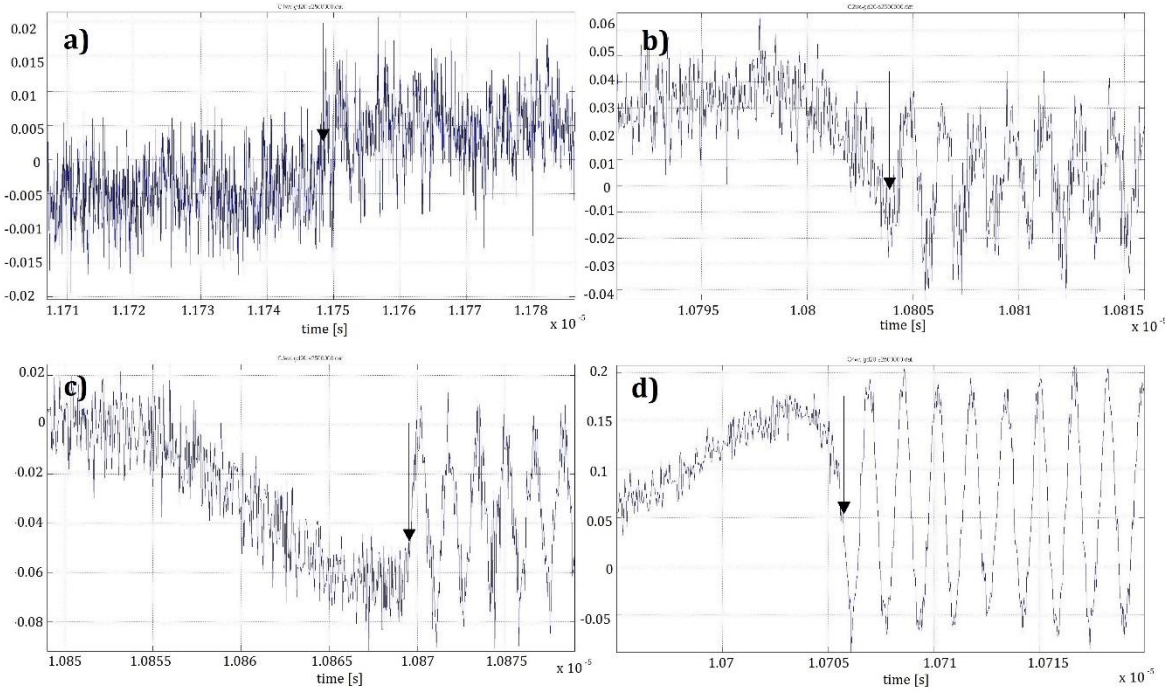

Figure 5.3. I Plot Signal: a) C1; b) C2; c) C3; d) C4.

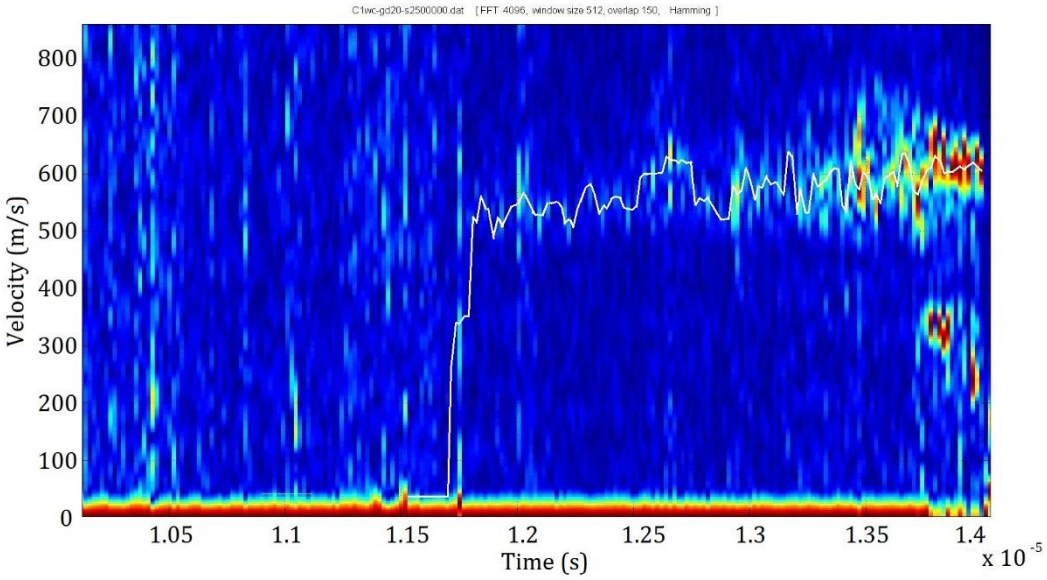

Figure 5.4. I C1 Spectrogram (velocity) interpolated within an area of interest.

5.2.2. Experiment II, impact at 320 m/s

One experiment was conducted at 320.3 m/s, approximately 320 m/s. The plot signals of all the sensors can be seen in Figure 5.5. The first graphic of the figure shows the intensity of the signal on C1. 12ns were given for tolerance, as the data registered some noise. The data of C2 and C4 is evident, however in C3 this is not as perceptive despite of the very meticulous analysis conducted and therefore it is believed that this sensor has failed. The sinusoidal pattern was not found on the span time of interest. For this reason, the average between C2 and C4 is taken as the correct value for the initial instant of time with a 2ns of error. The time of the propagation of the wave in the powder was about 0.9985μs, which, considering 1.018mm of thickness, accounts for a velocity of 866.34 m/s.

The velocity of the free surface of the powder is taken from Figure 5.6. On the spectrogram, an interpolation was made in the region of interest, which resulted in a well-defined function. The value of the velocity was taken based on the point where the slope of the curve is not accentuated and starts becoming uniform. It is estimated that the value is of approximately 303 m/s, with a tolerance of 15 m/s.

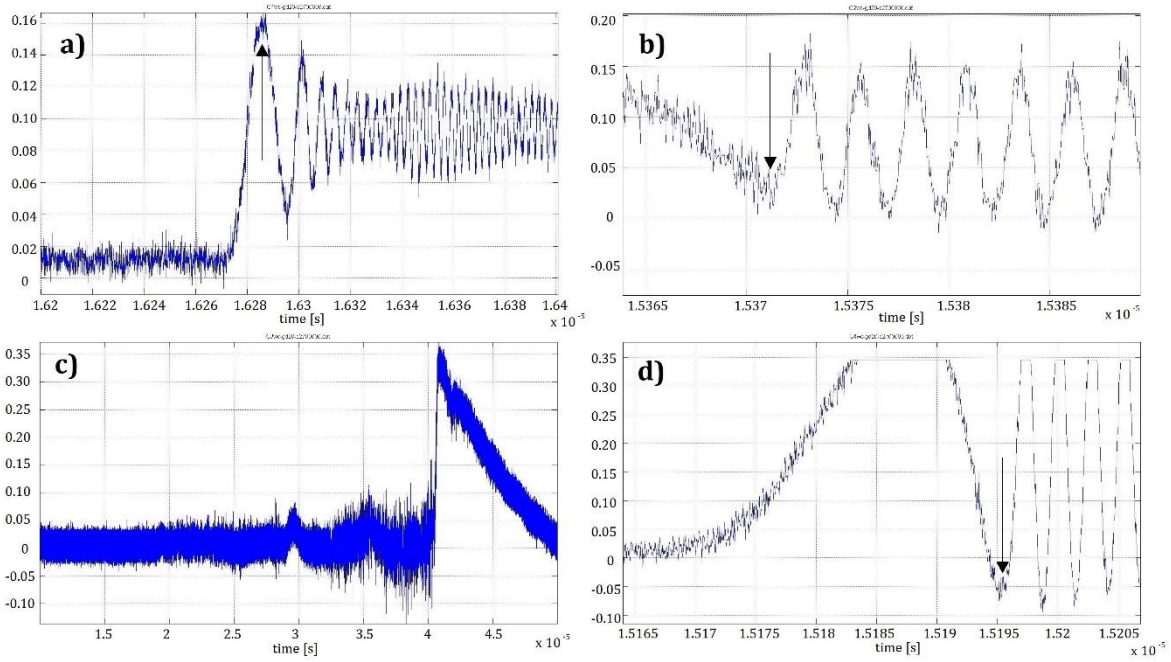

Figure 5.5. II Plot Signal: a) C1; b) C2; c) C3; d) C4.

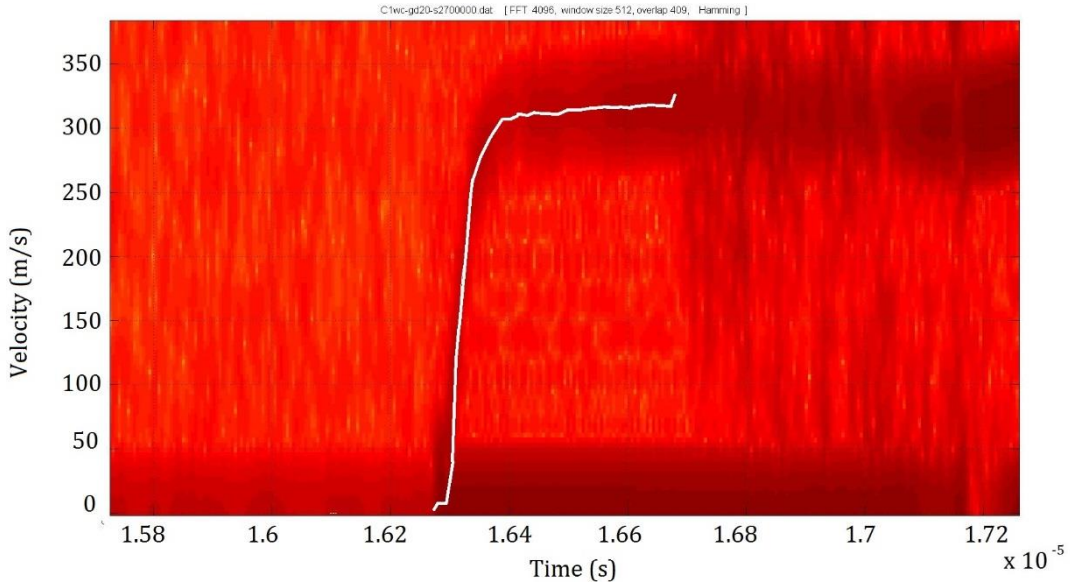

Figure 5.6. II C1 Spectrogram (velocity) interpolated within an area of interest.

5.2.3. Experiment III, impact at 660 m/s

One experiment was conducted at 659.2 m/s, approximately 660 m/s. The plot signals of all the sensors are displayed in Figure 5.7. All the data on this experiment is particularly good and it was also easier to define the values. The velocity of the wave was of approximately 1637.34 m/s, for a thickness of 0.97 and a span time of 0.59.

The velocity of the free surface of the powder is taken from Figure 5.8. Again, the velocity of the free surface of the material was taken after interpolating the function. It was considered a maximum error of 15 m/s for a velocity of 602 m/s.

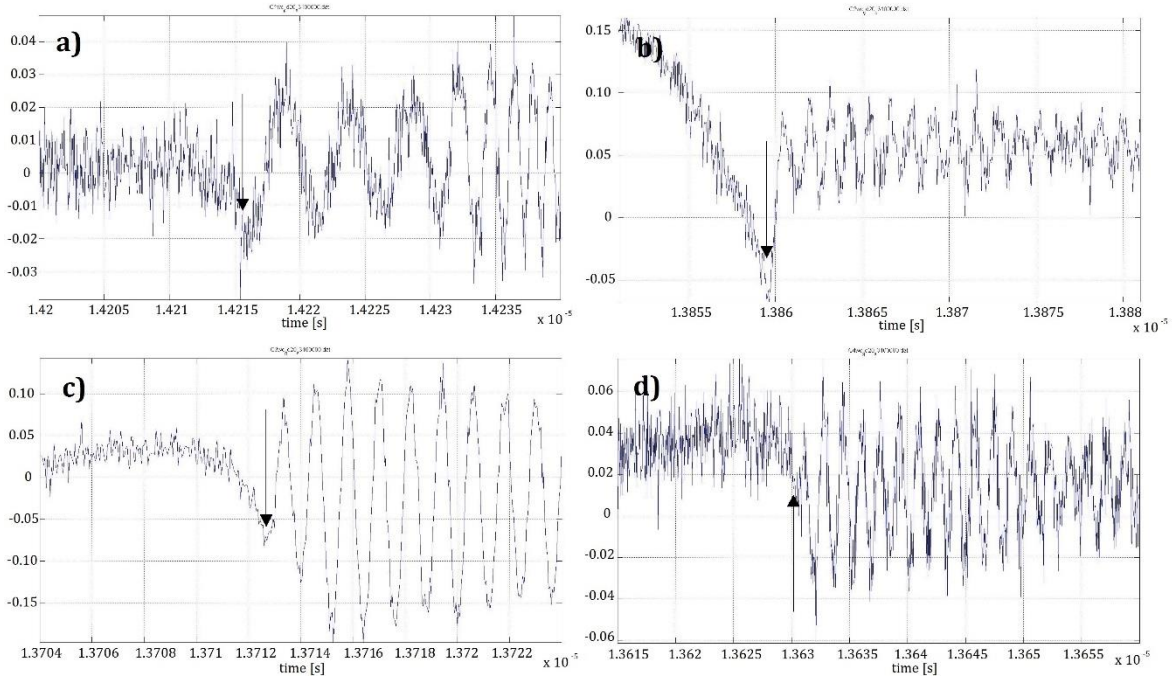

Figure 5.7. III Plot Signal: a) C1; b) C2; c) C3; d) C4.

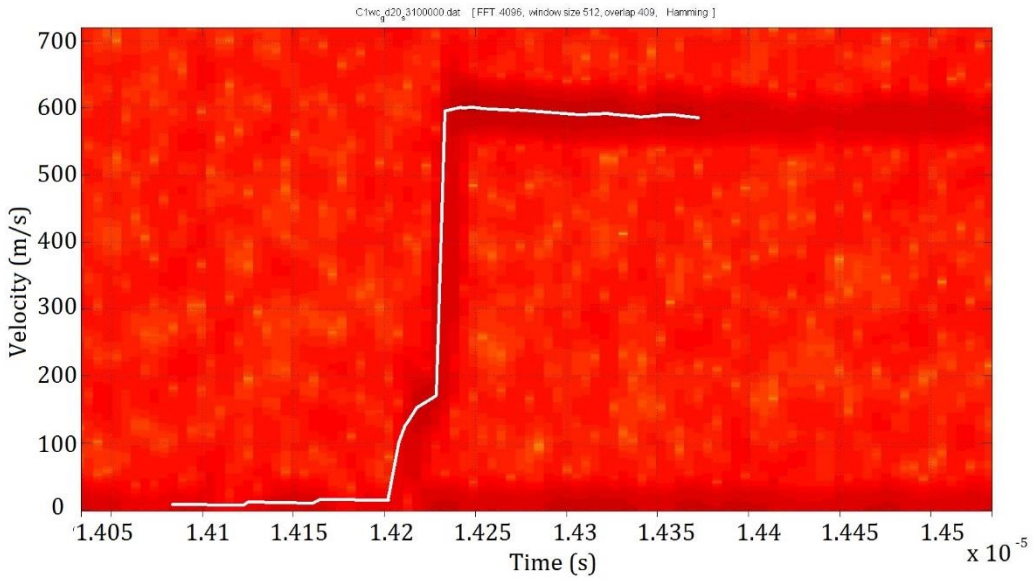

Figure 5.8. III C1 Spectrogram (velocity) interpolated within an area of interest.

5.3. Errors and the influence of tilt

The very small thickness of the samples used on this experiments, of approximately 1mm, made it possible to admit that the propagation of the shock wave would be perfectly planar. In fact, if the values of the sensor C2, C3 and C4 were analysed, an error can be found and previous theory cannot be fully verified. Despite of the high velocity and the small distance to the target, after leaving the barrel of the gun, the projectile tilts before the impact. This phenomena is not manipulated and it was tried to minimise its likelihood by proceeding with the alignment of the target. If the sabot impacts with tilt, the distance propagated through the waves is no longer correspondent to the thickness but a higher value. Despite this distance, it is admitted that thickness is the distance propagated by the shock and the arrival time of the shock wave is the average value of the three instants.

5.3.1. Propagation of errors

Once the experimental values are obtained, they are combined according to a formula, to reach the quantity desired. Even if the values register small inaccuracies, errors tend to propagate. Thus, the propagation of errors in the Hugoniot relations will be quantified in order to identify the influence they exert on the results. This "sum" of errors is calculated depending on the mathematical procedure, as it is shown in the following equations:

a) $z = x \pm y$

$$\Delta z = [(\Delta x)^2 + (\Delta y)^2]^{1/2} \tag{5.1}$$

b) $z = cxy$ or $z = c\frac{x}{y}$

$$\frac{\Delta z}{z} = \left[\left(\frac{\Delta x}{x}\right)^2 + \left(\frac{\Delta y}{y}\right)^2\right]^{1/2} \tag{5.2}$$

z is the resulting parameter and x and y the equating parameters, while Δz, Δx and Δy are the respective inaccuracies.

Figure 5.9 best describes the propagation of errors in the calculated parameters. The velocity of shock was chosen as an example, but the same logic may be used for all the variables according with their origin. The values of the velocity are taken from HetV data of the measuring experiments and dimensions of the samples.

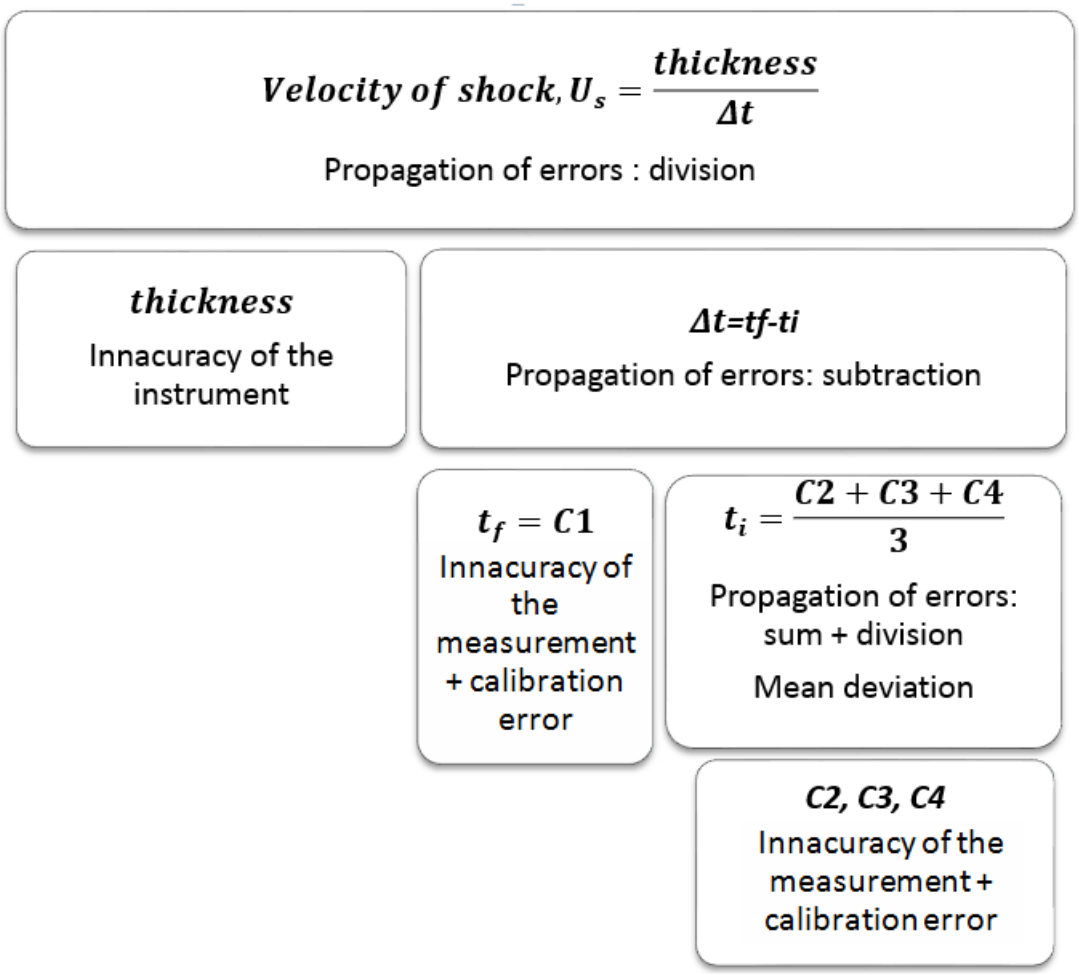

Figure 5.9. Scheme of the propagation of errors in Velocity of shock.

For obtaining more accurate results, the error of the arrival instant of the shock was calculated using the inaccuracy present on the data and the propagation of errors instead of the mean deviation. The inaccuracies of the instruments for were taken as it follows: $\Delta t=10^{-3}\mu s$; $\Delta m=10^{-3}g$; $\Delta x=10^{-3}mm$.

Table 5.3. Propagation of errors in the Hugoniot parameters.

	Inaccuracy					**Mean deviation**
Shots	U_s [m/s]	u_p [m/s]	ρ [g/cm^3]	P [GPa]	ν [cm^3/g]	t_i of Shock [μs]
I	5.512 (0.73%)	30 (5.77%)	0.00945 (0.94%)	0.280 (11.54%)	0.03246 (32.23%)	0.199
II	5.465 (0.63%)	15 (4.95%)	0.01227 (1.23%)	0.108 (9.91%)	0.02233 (22.59%)	0.088
III	11.877 (0.46%)	15 (2.5%)	0.01098 (1.10%)	0.239 (4.99%)	0.01452 (17.54%)	0.199

Regarding equations (2.3) and (2.6), in Table 5.3 it is visible a significant influence of the error in the pressure and specific volume. Due to the great precision of the HetV technique, the initial and final instants of the propagation of the wave in the material were clearly found, resulting in errors inferior to 1%. On the other hand, the velocity of the particle was measured with a minor error within 2 – 6%.

Resulting from the last three variables, pressure and specific volume register errors ranging from 5 to 12% and 17 to 32%, respectively. Both parameters are significantly changed by the inaccuracies of U_s and u_p and in experiment I it is easily perceptible where an inaccuracy of 30 m/s gives a maximum error of 32%, in the value of ν.

This variation of values is mostly explained by an uncontrollable error, the tilt of the projectile, since the measuring instruments have a great accuracy. On sample #27 (experiment II) not even the tilt is a possible cause, but also the brass back surface may be responsible for adding errors to the measurement. The fact that only three values of $P - \nu$ or $U_s - u_p$ are being analysed suggests that a small error in the data have an effect on the curves.

5.4. Hugoniot results

Before plotting the data into a graphic displaying the particle velocity *vs.* shock velocity, it is necessary to make an assumption. The velocity in situ of the particles is known

as half of the velocity on the free surface according to the free surface condition. Thus the following table resumes the data plotted on Hugoniot curve (Figure 5.10) which correlates the velocity of the shock with the particle velocity and its maximum pondered error as well results obtained by Vogler (2005).

Table 5.4. Hugoniot data in U_s-u_p plane.

Shot	Velocity of the shock [m/s]	Velocity of in situ particles [m/s]
I	1199.75	260.00
II	866.34	151.37
III	1618.85	300.77

Shock velocities for the experiments on WC powder are shown as function of particle velocity in Figure 5.10. Represented as a black line, a linear relationship between the velocities represents the data well over the range of these experiments. The best fit is given by:

$$U_s = 128.94 + 4.6313\, u_p \tag{5.3}$$

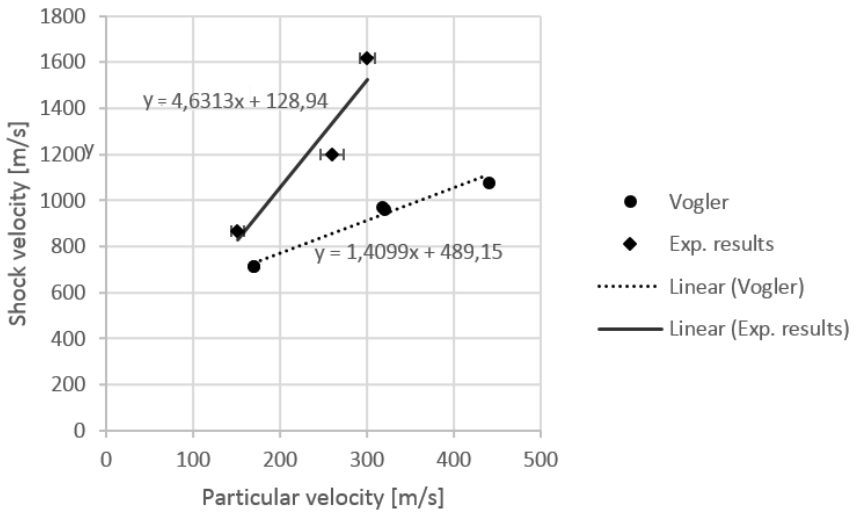

Figure 5.10. Hugoniot curve and pondered errors in the plane Us-up for the obtained experimental results and Vogler (2005).

According with the literature, the y-intercept is approximately the value of the sound speed on the material. It is well readily that in this case the referenced value is not approximately the velocity of the sound, taken as reference 489.15 m/s (Vogler, 2005). For lower values of the slope, the function lies on the previous assumption. Logically the errors are concentrated in the velocity of the shock wave, function of the measured times that can have errors.

The Hugoniot density can be calculated by using the relation in equation (2.3)

$$\rho = 8.655 \frac{128.94 + 4.6313\, u_p}{u_p} \tag{5.4}$$

where the value 8.655 is the average of the densities. The P – ν Hugoniot relation can be plotted as it is showed in Figure 5.11.

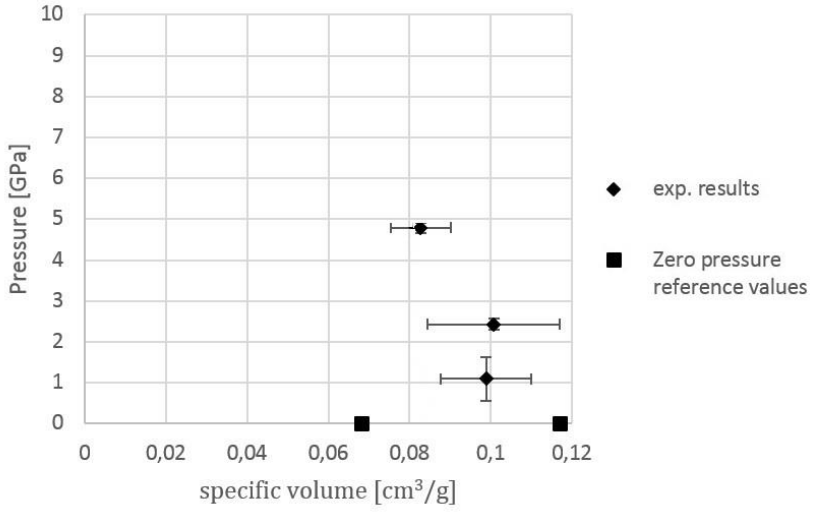

Figure 5.11. Hugoniot results and calculated propagation of errors in P – ν plane.

The following Table 5.5 is a resume of the data plotted in Figure 5.11.

Table 5.5. Hugoniot data in P-ν-plane.

Shot	Pressure [GPa]	Specific volume [cm³/g]
I	1.095	0.0988
II	2.426	0.1007
III	4.791	0.0828

5.5. Theoretical approaching

The prediction of the curves of the porous materials may be performed by using the Mie-Grüneisen model and the Thouvenin model. The experimental results are compared with the calculated curves to verify if there is a correlation in-between these models. This theoretical hypothesis distinctly bases on thermodynamic nature and shock propagation configuration foundations, as it was explained respectively in section 2.1.1.1 and.2.1.1.2.

5.5.1. Mie-Grüneisen model

An approximation of the Hugoniot curve of porous materials can be calculated using the Mie-Grüneisen equation, which relates the pressure with specific volume. This theory, was successful applied in previsingthe curve for porous materials such as tungsten (Boade, 1969 and Linde *et al.,* 1972), syntactic foams (Ribeiro, 2003) and copper (Boade, 1970) For this purpose, the constants C_0 and S of the Hugoniot curve of the solid material as well as the initial specific volume of the solid (ν_{s0}) and porous material (ν_{p0}) must be known.

For the present case, equation (2.24) was modified for:

$$P_{p1} = \frac{[2\nu_1 - \Gamma(\nu_{s0} - \nu_1)]c^2(\nu_{s0} - \nu_1)}{[2\nu_1 - \Gamma(\nu_{p0} - \nu_1)][\nu_{s0} - S(\nu_{s0} - \nu_1)]} \tag{5.5}$$

The information collected from measurements (section 3.2.2) gives that ν_{p0} is approximately 0.117cm^3/g, considering it as an average of the three values of measurements given in Table 3.2. Once more, ν_{s0} is 0.068 g/cm^3.

After a review based on the literature, the parameters of the curve could not be found for nickel-doped tungsten carbide. However, considered as an approximation, a pondered mean for 89% of WC and 11% of Ni was calculated for the desired parameters. Nickel's properties were taken as: $k = 180\ GPa; \rho = 8908\frac{Kg}{m^3}$; $c_v = 456\,J/(kg.K)$; $\alpha = 13 * 10^{-6}\,m/(m.K)$ $U_s = 4.59 + 1.44u_p$ (Marsh, 1980) and $C_b = 4590\ m/s$ (RFCafe). According to Grady (2009) neither shock velocity nor shock impedance is markedly affected by the variations in the composition, among the ceramics analysed on his report. On Figure 2.4 this statement is corroborated by the linear approximation of all the plotted experiments. Hence parameters of the curve Hugoniot of WC are taken as: $S = 1.31$ and $C_0 = 4.93\ km/s$. (Dandekar and Grady 1992). The remaining values for WC are $c_v = 961.6\,J/(kg.K)$, $k = 381.6\ GPa$ (Dandekar, 2001), $\alpha = 4.228\,m/(m.K)$ (Kurlov) and $C_b = 4930\,m/s$ (at

RFCafe website) The following table shows the values that were inserted in the equation (5.5).

Table 5.6. Mie-Grüneisen parameters.

$\nu_{0porous}$ [m3/kg]	ν_{0solid} [m3/kg]	C_0 [m/s]	S_0	C_b [m/s]	α [K^{-1}]	C_v [J/(kg.K)]	Γ
$1.170x10^{-4}$	$6.903x10^{-5}$	4892.6	1.3	4828.2	6.325×10^{-6}	905.984	0.584

On the following figure the interrupted line represents the curve for the Mie-Grüneisen model, whilst the plots figure the experimental results and the zero pressure point for an initial ν and fully compacted material.

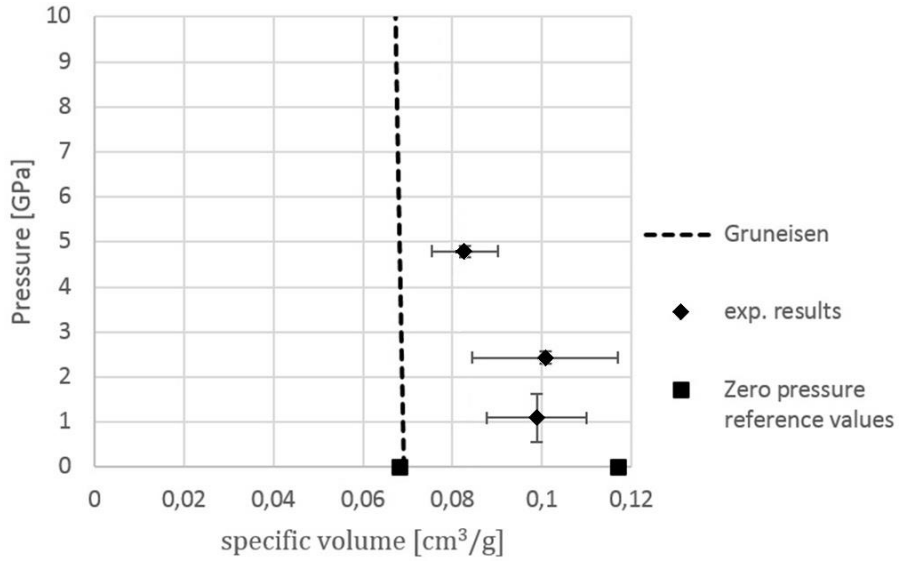

Figure 5.12. Mie-Grüneisen Model and experimental results and calculated propagation of errors in the P-ν.

5.5.2. Thouvenin model

The shock behaviour on powdered materials is regarded as a sequence of successive shocks between a set of plates, according with Thouvenin. The model has been used over the years as a prediction to the Hugoniot Curve of the materials. Authors such as Heyda (1968), Ribeiro et al. (2003 and (2009) and Kubota et al. (2014) successfully achieved their results.

The prevision for the Hugoniot curve is pictured in the following Figure 5.13.

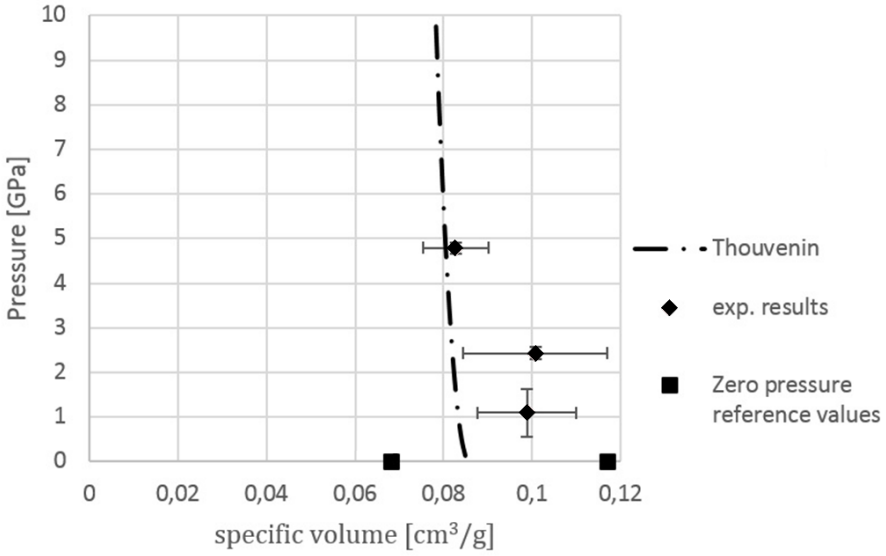

Figure 5.13. Thouvenin Model and experimental results and calculated propagation of errors in the P-ν.

The parameter λ, the inverse of porosity, was calculated using equation (2.26) regarding the same values of specific volume as in Table 5.6. Equations (2.27) and (2.28) calculates the velocity of the phase and shock using U_s and u_p given by the Hugoniot equation characterised by the terms C_0 and S_0 from Table 5.6. Once U_{sp} and u_{pp} are well characterised, Hoffman suggests the application of the conservation equations (2.4) and (2.6) to obtain the ν – *P* Hugoniot relation.

5.6. Discussion of the results and models

In Figure 5.12 and Figure 5.13 are depicted the graphics predicted by Mie-Grüneisen and Thouvenin /Hofmann models respectively. In fact, the experimental results do not perfectly lay down in none of the models, but Thouvenin's better describe their behaviour. According to Oh et al (Ribeiro, 2003), in the Gruneisen model, significant errors can be presented in the values of pressure, reflection of Γ coefficient, even if they are small. It is important to notice the Γ/ν was assumed as constant for Γ and ν values. From the analysis of the values of pressure and specific volume, it is noticeable that after the shock the material was not fully compressed owing to the velocity of the projectile that originated relatively low pressures. However, the point with highest velocity and pressure seems to be in concordance with the Thouvenin's curve, therefore the material was fully compacted by the shock.

After being quantified, the estimative of errors can be reflected on the experimental results in the Hugoniot curves. Results obtained by Vogler (2005) in WC powders are plotted in Figure 5.10 along with results from the present work. The values of velocity of sound in the material C_0 and the gradient S_0 are very different and neither the influence of a possible error changes the curve into a similarity between results.

In another point of view, on P-ν plane the inaccuracy on experimental points approaches the results to the curve predicted by Thouvenin model (Figure 5.13).

6. CONCLUSIONS AND FUTURE WORKS

A series of planar impact experiments using a gas gun were conducted on the ceramic Nickel-doped Tungsten Carbide powders for measuring the relation between the velocity of shock waves and particle velocity – the Hugoniot relation. A cylindrical flyer made of PMMA and pure cooper, was used to shock a target. This one was designed in accordance with the Heterodyne Velocimetry and consisted of a cylindrical cooper interface adjacent to the powdered sample compressed using an isostatic compressing dye. The impact between the moving flyer and the target resulted in the propagation of a shock wave that was quantified by means of four sensors, located next to the cooper and powder back interface. The velocity of the shock is calculated using the thickness of the sample and the difference between the final and initial instants, measured by the sensors. On the other hand, a sensor directly assessed the particle velocity of the sample by measuring the velocity of the free surface of the back surface of the specimen, found to be twice of the referenced velocity. Thus, the Hugoniot relation was characterised for different planes, using the two parameters of velocity obtained by analysing the data with a specific software. The experiments were performed at velocities at the projectile of 320, 500 and 620 m/s obtaining pressures in the range of 1.1 to 4.8 GPa. This stress created a shock with velocities of approximately 866 to 1620 m/s which imparted particle velocities between 151 and 300 m/s.

The design of the target revealed to be very practical and functional and the technique for preparing the optical fibres reliable, since the HetV measurement led to very precise results.

In the moment of impact the sabot collided with tilt which adds a small error to the results. This uncontrollable event generated different instants of time that were corrected the average value of the measurements instead.

Two models which from the Hugoniot relation of the non-porous material predicts the curve for porous material under study, were reviewed and used for comparison with experimental results. Although none of the models perfectly describes the results, data suggests that the material was not fully compacted for the impacts of lower velocities. In

fact, if this issue is considered, in addition to errors calculated to quantify the inaccuracy of the measurements, experimental results can approximately fit the curve of Thouvenin model.

For future works it is suggested a study the Hugoniot relation of GD20N powders for higher velocities, as well the characterisation of other WC-Ni powders with different percentages of Ni for posterior comparison of results. An improvement of the measurement/ quantification of the tilt of the sabot and a comparison between a similar setup with a transparent back window, for directly measuring the particle velocity, is also a suggested task for the future.

BIBLIOGRAPHY

Amulele, G. M., Manghnani, M. H., Marriappan, S., Hong, X., Li, F., Qin, X., Liermann, H. P., (2008) "Compression behavior of WC and WC-6%Co up to 50 GPa. Determined by Synchrotron X-Ray Diffraction and ultrasonic technique", J. Appl. Phys., 103, 1.

Boade, R., 1969, "Dynamic compression of porous tungsten", Journal of Applied Physics, vol. 40, nº9, pp. 3781-3785

Boade, R. 1970, "Principal-Hugoniot, second-shock Hugoniot and release behavior of pressed cooper", Journal of Applied Physics, vol. 41, nº11, pp. 4542-4551.

Bulk sound speed of materials, searched in 20th of August at http://www.rfcafe.com

Dandekar, P. D., 2001, "Shock response of Boron carbide", Weapons and materials research directorate, ARL

Dandekar, P. D., Grady, D., E., "Shock equation of state and dynamic strength of tungsten carbide, AIP Conference proceedings 620, 783 (2002).

Gourdin, W.H. (1986), "Dynamic consolidation of metal powders", In: Progress in materials science, Vol. 30, 30-39.

Grady, D. E. (1995), "Dynamic Properties of Ceramic Materials" Sandia National Laboratories Technical Report, SAND94-3266, February.

Grady, D. E., (1999), "Impact Failure and Fragmentation Properties of Tungsten Carbide", Int. J. Impact Eng. 23, 307-317.

Grady, D. E., (2009), "Analysis of shock and high-rate data for ceramics: Equation of state properties and fragmentation in the ballistic environment, Applied Research Associates, Inc.

Hayes, D. B., (1973), "Introduction to stress wave phenomena", SLA-73-0801

Herrmann, W., 1969, "Constitutive equation for the dynamic compaction of ductile porous materials", Journal of Applied Physics, 40, pp: 2490-2499

Heyda, J., F., 1968, "Plate-gap model of a porous solid and its application to impact by reduced density projectiles", NASA contractor report, NASA CR - 1140

History of Weimar republic, Searched in 4th of April at http://www.thyssenkrupp.com

Hofmann, R., Andrews, D., Maxwell, D., 1968, "Computed shock response of porous aluminum, Journal of Applied Physics 39, pp: 4555-4562.

Kubota, S., Saburi, T., Ogata, Y., Wada, Y., Nagayama, K., 2014, "Experiments and numerical simulations of plate gap model for high energetic materials", Journal of physics: Conf. Ser. 500 052022

Kumar, Sanjay, Singh, Kulbir, Saxena, Rajiv, (2011), "Analysis of Dirichlet and generalized Hamming window functions in the fractional Fourier transform domains", Signal processing 91, pages 600 to 606

Kurlov, A. S., Gusev, A. I., "Tungsten carbides: structure, properties and application in hardmetals", Dordretch: Springer 2013

Linde, R., Seaman, L., Schmidt, D., 1972, "Shock response of porous copper, iron, tungsten and polyurethane", Journal of applied Physics, vol. 43, nº8, pp 3367-3375

Marsh, S., P., 1980, "LASL shock Hugoniot data", University of California Press, Berkeley, EUA.

McQueen, R. G., Marsh, S. P., Taylor, J. W., Fritz J. N., Carter, W. J., (1970), "The Equation of State of Solids from Shock Wave Studies, In High Velocity Impact Phenomena", R Kinslow ed., Academic Press

Pires, A. S. (2012) "Aplicação da compactação por explosivos na produção de compósitos de carboneto de tungsténio". Doctor thesis in Cience and Engineering of materials at University of Aveiro.

Pruemmer, R. A., Bhat, T. B., Kumar, K. S. and Hokamoto, K. (2006), "Explosive Compaction of Powders & Composites", CRC Press, 2-16

Ribeiro, J., Mendes, R., Plaksin, I., Campos, J., Capela, C., 2009, "High pressure range shock wave data for syntactic foams", AIP conference proceedings 1195

Ribeiro, J., Campos, J., 2003, "Shock behavior of syntactic foams", Manufacture, testing and utilization of light- weight armour materials, Vol. 1, pp. 75-133

Rice University, Houston. "Error analysis and significant figures" visited in 10th of May,at http://owlnet.rice.edu

Ribeiro, J. B. (2003) "Propagação de ondas de choque em espumas sintácticas". Doctor thesis in Mechanical Engineering at University of Coimbra

Shon, I., J., Jeong, I. K., Ko, I. Y., Doh, J. M., Woo, K. D., (2007), "Sintering behavior and mechanical properties of WC-10Co, WC-10Ni and WC-10Fe hard materials produced by high-frequency induction heated sintering", Ceramics international 35 (2009) 339-344

Strand, O. T., Berzins, l. V.., Goosman, D. R., Kuhlow W. W., Sargis, P. D., Whitworth, T. L. (2004), "Velocimetry Using Heterodyne Techniques", UCRL-CONF-206034

Thouvenin, J., 1965, "Effect of a shock wave on a porous solid", Fourth International Symposium on detonation, ACR-126, Office of Naval Research, Department of the Navy, Washington DC, EUA pp 258-265

Vogler, T. J., Gluth, J. W., Grady, D. E., (2005), "Dynamic compaction of Tungsten Carbide Powder", Sandia National Laboratories.

Winter, R. E., (2009), "Key concepts of shock hydrodynamics", AWE report 881/09, Imperial college

APPENDIX A

2D Project of the isostatic pressing dye

A.1. Body part I

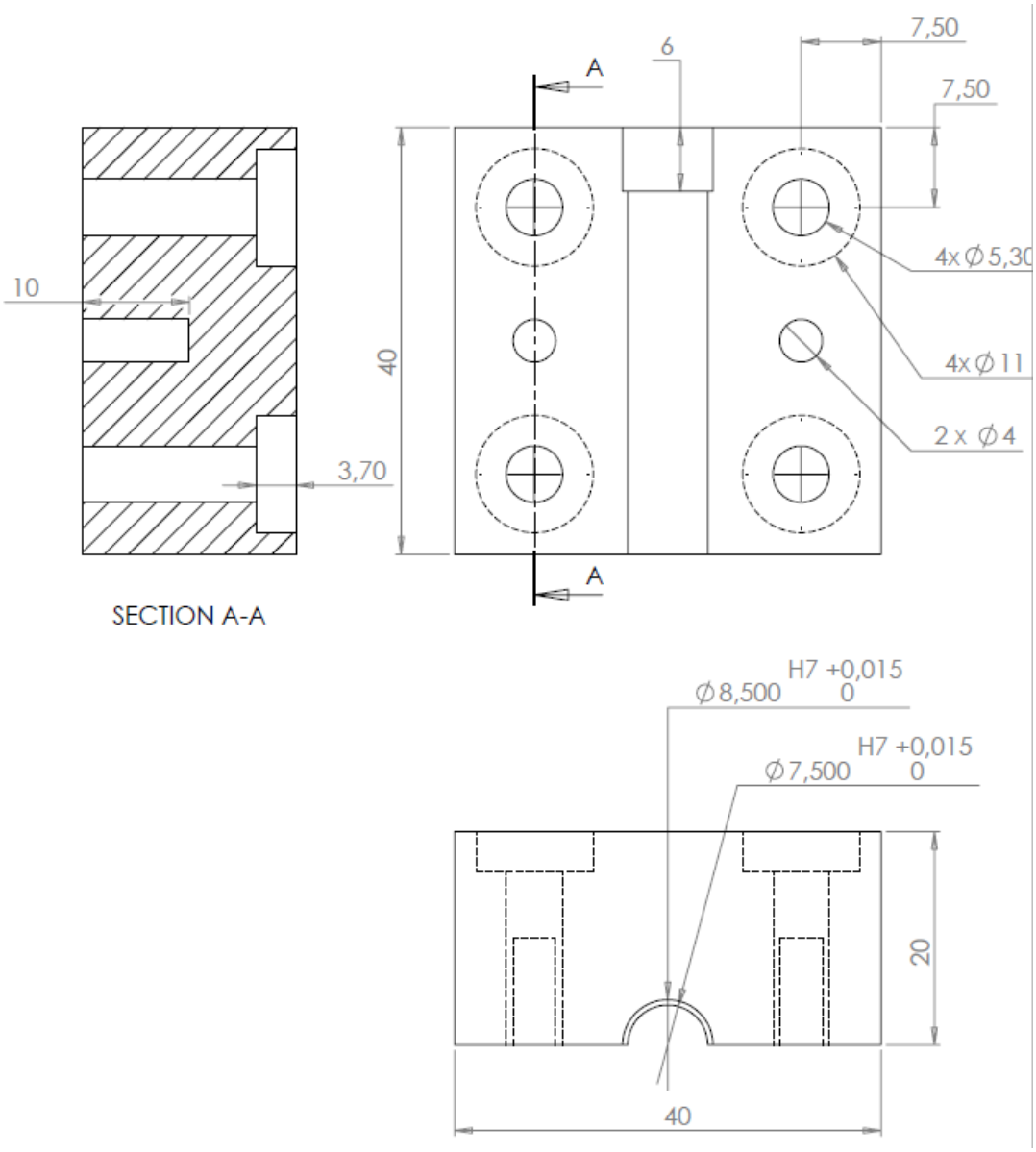

A.2. Body part II

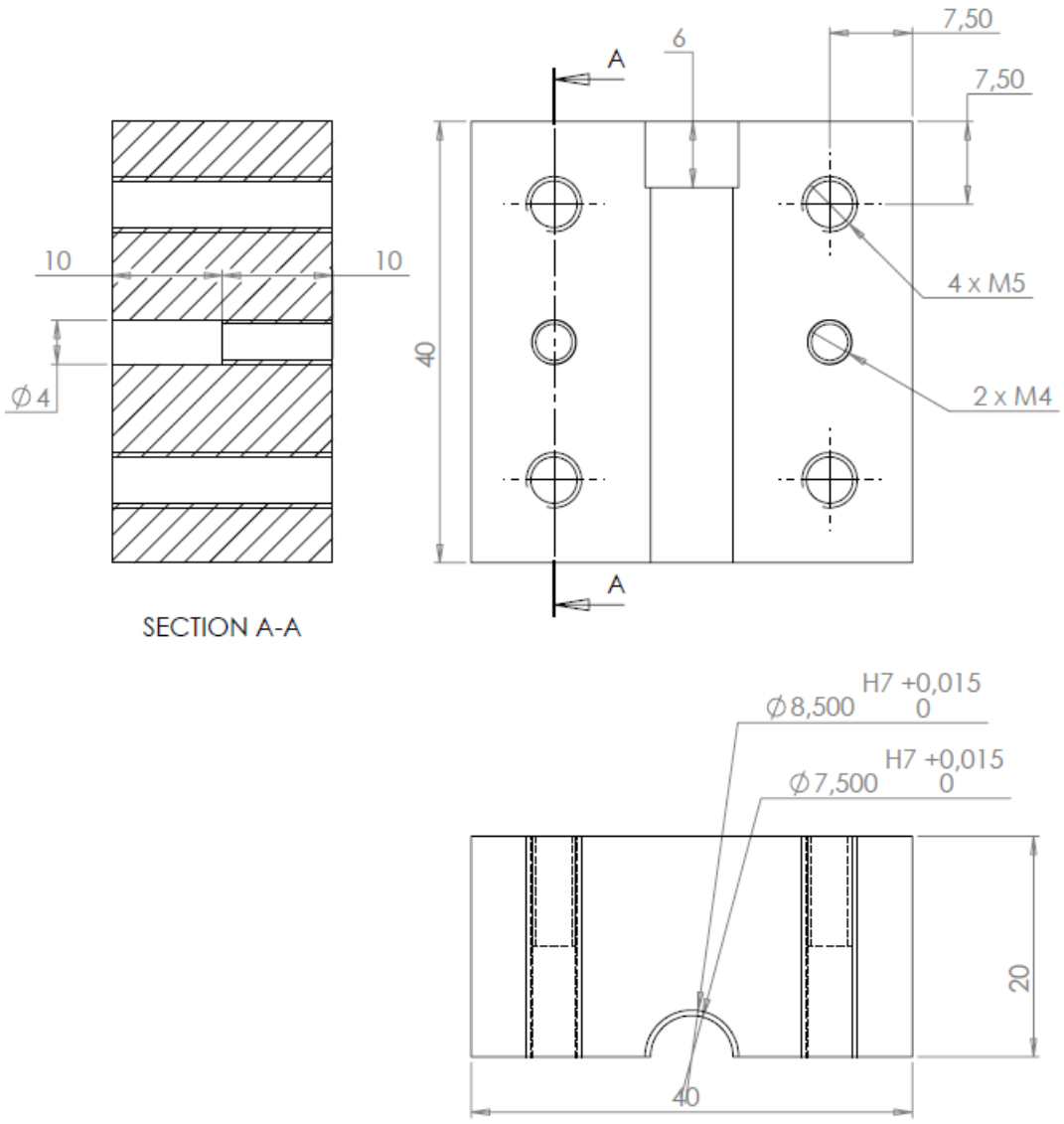

A.3. Punch

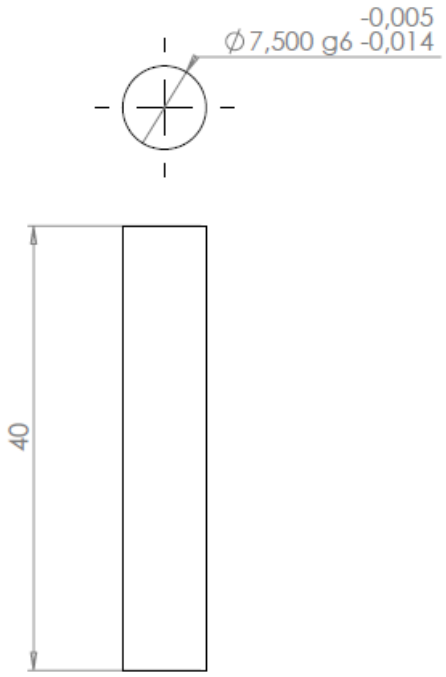

A.4. Base

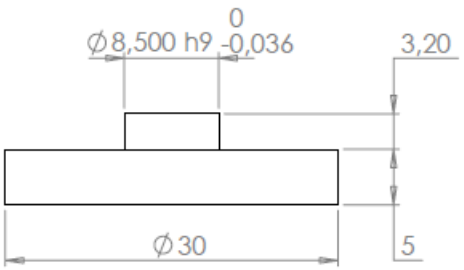

APPENDIX B

2D project of the target

B.1. Cooper plate

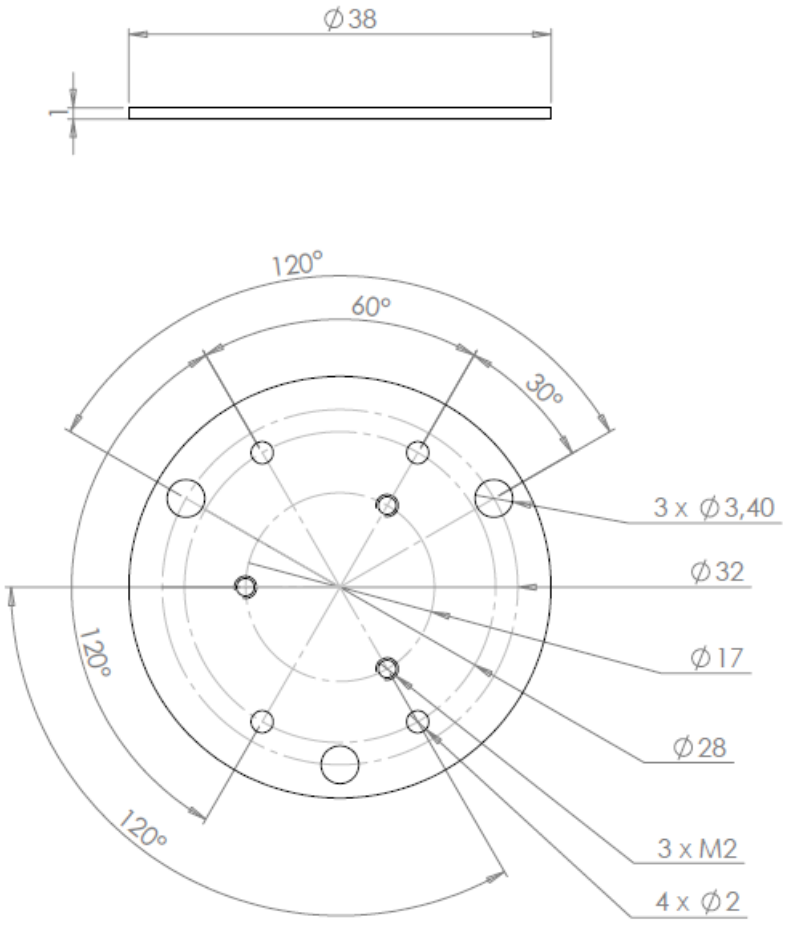

B.2. Sample holder

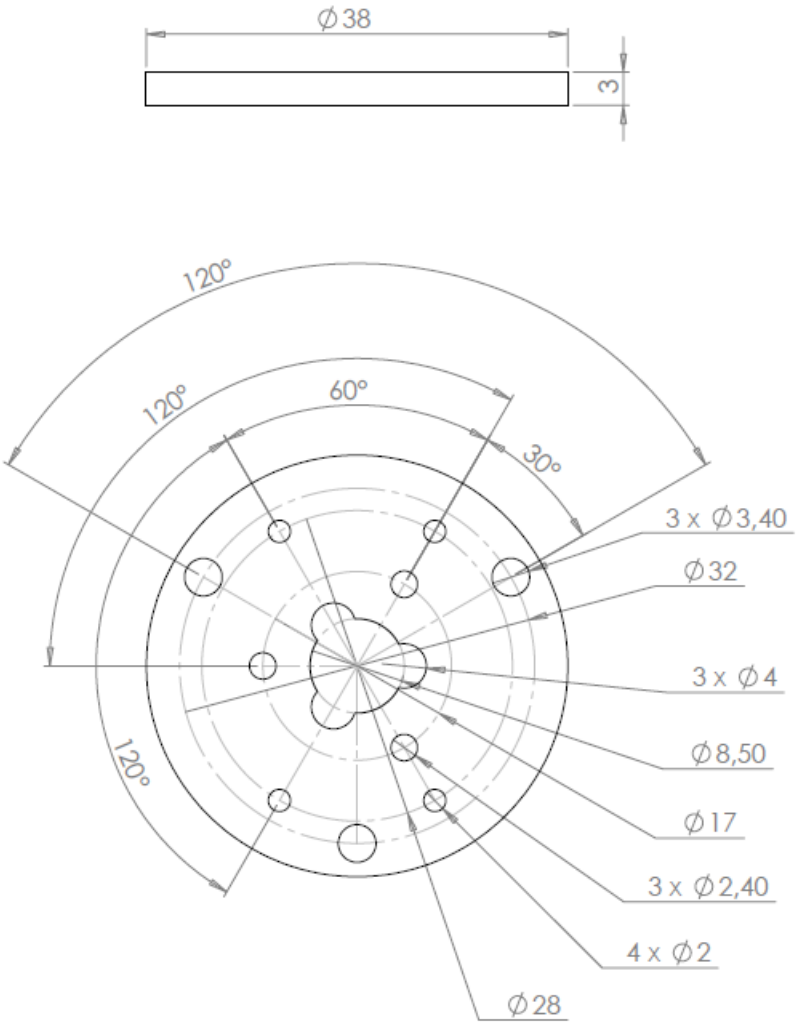

B.3. Fiber holder

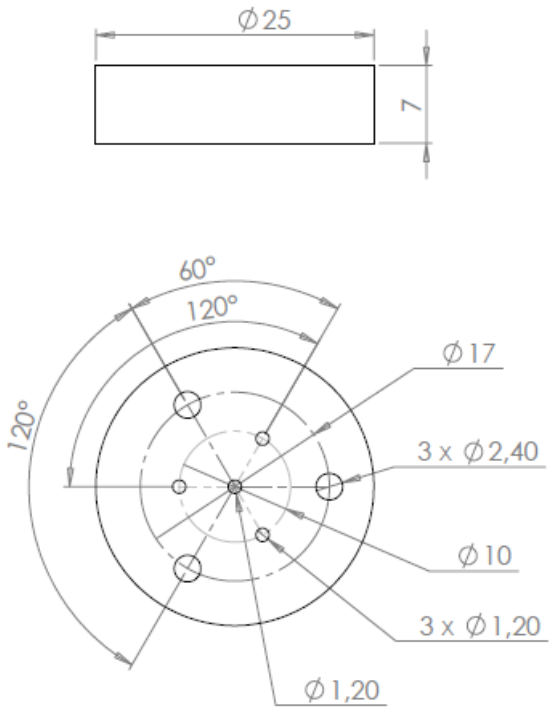

B.4. Ring